

# Instability of non-supersymmetric smooth geometries

Vitor Cardoso\*

*Department of Physics and Astronomy, The University of Mississippi, University, MS 38677-1848, USA* †

Óscar J. C. Dias,‡ Jordan L. Hovdebo,§ and Robert C. Myers¶

*Perimeter Institute for Theoretical Physics,  
Waterloo, Ontario N2L 2Y5, Canada*

and

*Department of Physics, University of Waterloo,  
Waterloo, Ontario N2L 3G1, Canada*

Recently certain non-supersymmetric solutions of type IIB supergravity were constructed [1], which are everywhere smooth, have no horizons and are thought to describe certain non-BPS microstates of the D1-D5 system. We demonstrate that these solutions are all classically unstable. The instability is a generic feature of horizonless geometries with an ergoregion. We consider the endpoint of this instability and argue that the solutions decay to supersymmetric configurations. We also comment on the implications of the ergoregion instability for Mathur’s ‘fuzzball’ proposal.

## I. INTRODUCTION

String theory has made great progress in understanding the microphysics of black holes. In particular, for certain (nearly) supersymmetric black holes, one is able to show that the Bekenstein-Hawking entropy  $S_{\text{BH}} = A_{\text{hor}}/4G$ , as computed in the strongly-coupled supergravity description, can be reproduced in a weakly-coupled D-brane description as the degeneracy of the relevant microstates [2] — for reviews, see [3]. The AdS/CFT correspondence [4] provides further insights into these issues by providing a dictionary relating the geometric description of the physics in the near-horizon region with the physics of a dual conformal field theory — see [5] for a review. In particular, the AdS/CFT indicates that Hawking evaporation should be a unitary process, in keeping with the basic tenets of quantum theory. The discussion of black holes in the context of the AdS/CFT correspondence makes evident that the path integral over geometries in the bulk may include multiple saddle-points, *i.e.*, several classical supergravity solutions, as found *e.g.*, in [6–8].<sup>1</sup> Another point that was realized early on is that the geometric description of individual microstates would not have a horizon [9, 10].

In recent years, Mathur and collaborators have incorporated these ideas in a radical revision of the stringy description of black holes — for a review, see [11]. They argue that each of the CFT microstates corresponds to a separate spacetime geometry with no horizon. The black hole is dual to an ensemble of such microstates and so the black hole geometry only emerges in a coarse-grained description which ‘averages’ over the  $e^{S_{\text{BH}}}$  microstate geometries. In particular, this averaging should produce an effective horizon at a radius where the individual microstate geometries start to ‘differ appreciably’ from one another [12, 13]. Therefore in this scenario, quantum gravity effects are not confined close to the black hole singularity, rather the entire interior of the black hole is ‘filled’ by fluctuating geometries — hence this picture is often referred to as the ‘fuzzball’ description of black holes. The first support for this proposal came from finding agreement between the propagation time of excitations in the throat of certain microstate geometries and in the dual brane description [13, 14]. A further remarkable feature, that has drawn attention to these ideas, is that there is growing evidence that the microstate geometries may be smooth, as well as horizon-free.<sup>2</sup> In the case of the D1-D5 system, smooth asymptotically flat geometries can be constructed corresponding to all of the RR ground states in the dual CFT [13, 15]. Despite their large degeneracy, this two-charge system will not produce a macroscopic black hole horizon. However, a large horizon can be produced by introducing a third charge, Kaluza-Klein momentum

---

† Also at: Centro de Física Computacional, Universidade de Coimbra, P-3004-516 Coimbra, Portugal

\*Electronic address: [vcardoso@phy.olemiss.edu](mailto:vcardoso@phy.olemiss.edu)

‡Electronic address: [odias@perimeterinstitute.ca](mailto:odias@perimeterinstitute.ca)

§Electronic address: [jlhovdeb@sciborg.uwaterloo.ca](mailto:jlhovdeb@sciborg.uwaterloo.ca)

¶Electronic address: [rmyers@perimeterinstitute.ca](mailto:rmyers@perimeterinstitute.ca)

<sup>1</sup> Of course, in these examples, a single saddle-point typically dominates the path integral.

<sup>2</sup> ‘Smooth’ means the curvature is finite everywhere up to orbifold singularities. The curvatures in the throat may also be very large.

[16, 17]. Recently progress has been made in constructing smooth microstate geometries in the D1-D5-P system [18–20]. While large families of such solitons are now known, a complete understanding of the three-charge case remains to be found. Further preliminary work on the four charge system of D1-D5-P-KK has also appeared [21].

In general, the preceding discussion connecting microstates with smooth geometries focuses on supersymmetric configurations. This raises the interesting question of how the fuzzball proposal would be extended to non-supersymmetric black holes. In particular, are there non-supersymmetric versions of the smooth horizon-free geometries corresponding to non-BPS microstates? Remarkably, Jejjala, Madden, Ross and Titchener [1] recently extended the known set of D1-D5 microstate geometries with a family of non-supersymmetric solutions, hereafter referred to as JMaRT solitons. The JMaRT solutions comprise a five-parameter family of non-supersymmetric smooth geometries which are asymptotically flat.<sup>3</sup> These solutions may be parameterized by the D1-brane and D5-brane charges, the (asymptotic) radius of the internal circle with Kaluza-Klein momentum, and by two integers  $m$  and  $n$  which fix the remaining physical parameters. These integers also determine a spectral flow in the CFT which allows the underlying microstate to be identified. For  $m = n + 1$ , the JMaRT solitons reduce to supersymmetric solutions found previously in [15, 18, 19].

An important feature which distinguishes the JMaRT solitons from any of the analogous supersymmetric solutions is the presence of an ergoregion. As a consequence, in these non-supersymmetric geometries, there is an inner region (that extends to the origin) where states of negative energy are allowed. This then leads naturally to the question of whether or not the ergoregion produces an instability of the background. One possibility is that the ergoregion may lead to superradiant scattering which can produce a catastrophic instability in some situations [22–24]. However in the present case, this possibility is easily dismissed [1] because the solutions are horizon-free. Since the seminal work of Zel’dovich [25] on superradiant amplification of electromagnetic waves incident upon an absorbing cylinder, it has been known that the key ingredients for superradiance is the existence of an ergoregion *and* an absorbing surface. For black holes, the horizon plays the latter role but certainly the JMaRT geometries lack such a surface.

Quite interestingly, there is another class of instabilities, which we simply refer to as ‘ergoregion instabilities’, that generically afflict spacetime geometries with an ergoregion, but no horizon. These instabilities were first discovered by Friedman [26], who provided a very general discussion. Explicit computations of the instability were later made in [27, 28] for the case of rotating stars with an ergoregion. There the existence of this instability was explicitly verified for a free scalar field in the background of a rotating star. According to Friedman’s general arguments however, the instability should also exist for electromagnetic and gravitational waves. Since the JMaRT solutions [1] have an ergoregion but no horizon, one might suspect that a similar ergoregion instability would arise in these geometries. The present paper then explicitly verifies the presence of an ergoregion instability for the JMaRT backgrounds with a variety of techniques. Further we consider the endpoint of the resulting decay and argue that it should be a smooth supersymmetric solution.

Our results have immediate consequences for the endpoint of tachyon decay discussed in [29]. There, Ross extended the discussion of [30] to D1-D5 black strings for which he identified tachyonic string modes in a particular winding sector. He argued that the condensation of these tachyons would transform the spacetime to a JMaRT soliton. In conjunction with the above results, we see that these solutions cannot be the final endpoint of these decays but rather they should end with a supersymmetric microstate geometry. Our analysis and the ergoregion instability may also have interesting implications for Mathur’s fuzzball proposal more generally.

The remainder of our paper is organized as follows: Section II provides a brief exposition on Friedman’s analysis [26]. In Section III, we briefly review some of the features of the JMaRT solutions and present the main equations used in the subsequent analysis, namely the radial and angular wave equations for a free massless scalar field, as well as some of their properties. In Section IV we compute the details of the instability using a WKB approach [27]. We show explicitly that the instability exists for a general non-supersymmetric geometry of [1], and that it disappears for supersymmetric objects, as expected. In Section V, we use an alternative method, that of matched asymptotic expansions, to investigate the instability and its properties. The methods of sections IV and V are complementary, *i.e.*, their regime of validity is different. We then perform a numerical analysis of the wave equation in Section VI to complement the analytical calculations. We find that the results of both analytical analyses agree remarkably well with the numerical results. In section VII, after summarizing the main properties of the ergoregion instability, we discuss various related topics: the endpoint of this instability; its consequences for Ross’s tachyon condensation [29]; general implications for the fuzzball picture of black holes.

---

<sup>3</sup> By considering orbifolding, this family can be extended by a third integer [1] but we will focus on the original five-parameter solutions.

## II. ERGOREGION INSTABILITIES

There are two classes of instabilities that are of potential interest for the JMaRT backgrounds [1] (or non-supersymmetric geometries in general), namely: the superradiant instability, and the ergoregion instability. In this section, we demonstrate why superradiance is not present in these geometries, as first noted in [1], and we introduce the general argument of [26] that suggests an ergoregion instability is present. In the following sections, we verify the presence of the ergoregion instability with a complete analytic and numerical analysis of its properties.

### A. Geometries with an ergoregion and horizon: Superradiance

For a general (stationary asymptotically flat) black hole, the equations describing spin- $s$  fields can always be written as

$$\frac{d^2\Psi}{dr_*^2} + V(\omega, r)\Psi = 0 \quad (1)$$

where  $\omega$  was introduced with a Fourier transform with respect to the asymptotic time coordinate:  $\Psi(t) = e^{-i\omega t}\Psi(\omega)$ . The radius  $r_*$  is a convenient tortoise coordinate and in general one finds:

$$\begin{cases} r_* \sim r, & V \sim \omega^2 & \text{as } r \rightarrow \infty, \\ e^{r_*} \sim (r - r_+)^{\alpha}, & V \sim (\omega - \Phi)^2 & \text{as } r \rightarrow r_+, \end{cases} \quad (2)$$

where  $\alpha$  is a positive constant. The potential  $\Phi$  can be a rotational potential (in the Kerr geometry  $\Phi = m\Omega$ , with  $m$  an azimuthal number, and  $\Omega$  the angular velocity at the horizon) or a chemical potential (in the Reissner-Nördstrom geometry,  $\Phi = qQ$ , where  $q$  is the charge of the field and  $Q$  the charge of the black hole).

For a wave scattering in this geometry, Eq. (1) yields the following asymptotic behavior:<sup>4</sup>

$$\Psi_1 \sim \begin{cases} \mathcal{T}(r - r_+)^{-i\alpha(\omega - \Phi)} & \text{as } r \rightarrow r_+, \\ \mathcal{R}e^{i\omega r} + e^{-i\omega r} & \text{as } r \rightarrow \infty. \end{cases} \quad (3)$$

These boundary conditions correspond to an incident wave of unit amplitude from  $+\infty$  giving rise to a reflected wave of amplitude  $\mathcal{R}$  going back to  $+\infty$  and a transmitted wave of amplitude  $\mathcal{T}$  at the horizon — the boundary condition introduces only ingoing waves at the horizon. Assuming a real potential (which is almost always the case) the complex conjugate of the solution  $\Psi_1$  satisfying the boundary conditions (3) will satisfy the complex-conjugate boundary conditions:

$$\Psi_2 \sim \begin{cases} \mathcal{T}^*(r - r_+)^{i\alpha(\omega - \Phi)} & \text{as } r \rightarrow r_+, \\ \mathcal{R}^*e^{-i\omega r} + e^{i\omega r} & \text{as } r \rightarrow \infty. \end{cases} \quad (4)$$

Now, these two solutions are linearly independent, and the standard theory of ODE's tells us that their Wronskian,  $W = \Psi_1\partial_{r_*}\Psi_2 - \Psi_2\partial_{r_*}\Psi_1$ , is a constant (independent of  $r$ ). If we evaluate the Wronskian near the horizon, we get  $W = -2i(\omega - \Phi)|\mathcal{T}|^2$ , and near infinity we find  $W = 2i\omega(|\mathcal{R}|^2 - 1)$ . Equating the two we get

$$|\mathcal{R}|^2 = 1 - \frac{\omega - \Phi}{\omega}|\mathcal{T}|^2. \quad (5)$$

Now, in general  $|\mathcal{R}|^2$  is less than unity, as is to be expected. However, for  $\omega - \Phi < 0$  we have that  $|\mathcal{R}|^2 > 1$ . Such a scattering process, where the reflected wave has actually been amplified, is known as superradiance. Of course the excess energy in the reflected wave must come from that of the black hole, which therefore decreases.

Superradiant scattering can lead to an instability if, *e.g.*, we have a reflecting wall surrounding the black hole that scatters the returning wave back toward the horizon. In such a situation, the wave will bounce back and forth, between the mirror and the black hole, amplifying itself each time. The total extracted energy grows exponentially until finally the radiation pressure destroys the mirror. This is Press and Teukolsky's black hole bomb, first proposed in [22]. This instability can arise with an effective 'mirror' in a variety of situations: a scalar field with mass  $\mu > \omega$  in a Kerr background creates a potential that can cause flux to scatter back toward the horizon [31]; infinity in asymptotically AdS spaces also provides a natural wall [32] that leads, for certain conditions, to an instability; a wave propagating around rotating black branes or rotating black strings may similarly find itself trapped [33].

---

<sup>4</sup> Implicitly, we consider a massless field here but the discussion is generalized to massive fields in a straightforward way.

## B. Geometries with ergoregion but horizon-free: Ergoregion instability

Suppose now there is no horizon in the background spacetime. What changes with respect to the former discussion is the boundary conditions: since there is no horizon and no absorption. For this case, the boundary condition (3) at the horizon is replaced by some kind of regularity condition at the origin. We suppose the radial coordinate  $r$  now ranges from zero to infinity and we impose the following boundary condition:

$$\Psi \sim Af(r), \quad r \rightarrow 0, \quad (6)$$

where  $f(r)$  is some well-behaved *real* function. This ansatz encompasses for instance typical regularity requirements where, *e.g.*, one chooses  $f(r) \sim r^\beta$  with  $\beta > 0$ . Repeating the above calculation, one gets  $|\mathcal{R}|^2 = 1$ . Therefore the absence of a horizon, which precludes any absorption, prevents superradiance and hence the superradiant instability.

Nevertheless, geometries with an ergoregion but without horizons are the arena of another class of instability. This ergoregion instability was discovered by Friedman [26]. Even though his discussion was made in four-dimensions only, it is trivial to extend it to any number of dimensions. The instability arises because of the following [26]: Given the test field energy-momentum tensor  $T^{ab}$ , we can associate a canonical energy

$$\mathcal{E}_S = \int_S t^a T_a^b dS_b, \quad (7)$$

where  $t^a$  is the background Killing vector which generates time translations in the asymptotic geometry. Now, because  $t^a$  is space-like within an ergosphere, initial data can be chosen on a Cauchy surface  $S$  which makes  $\mathcal{E}_S$  negative. Moreover, it is shown in [26] that the energy can be negative only when the test field is time dependent. Then, since the field is time dependent, and since only positive energy can be radiated at future null infinity, the value of  $\mathcal{E}_S$  can only decrease further from one asymptotically null hypersurface  $S$  to another, say,  $S'$ , in the future of  $S$ . Thus, the energy  $\mathcal{E}_S$  will typically grow negative without bound. This instability was computed analytically using a WKB approximation in [27] for rotating stars. There it was shown that the instability timescale is usually very large (typically larger than the age of the universe). The analysis of [27] was improved in [28] where further details of the instability were computed numerically.

A key assumption above is that the system can not settle down to a negative energy configuration which, while time dependent, is nonradiative. Friedman [26] was able to rule out such marginal cases where  $\mathcal{E}_S$  is negative but constant for a four-dimensional massless scalar or electromagnetic fields. However, in fact, one is able to identify negative energy bound states for the JMaRT backgrounds — see Appendix D — and so a more thorough analysis is called for. Hence, in the following, we apply a variety of techniques to explicitly show that these microstate geometries suffer from an ergoregion instability.

## III. FORMALISM

We now consider wave propagation of a free massless scalar field in the JMaRT backgrounds [1], and from this identify an ergoregion instability for these geometries in the subsequent sections. The JMaRT solutions are described in detail in [1] and are quite involved. We will provide a brief discussion of some of the properties of these solutions here, but will refer the reader to [1] for the full details.

The JMaRT solitons are solutions of type IIb supergravity corresponding to three-charge microstate geometries of the D1-D5-P system. The system is compactified to five dimensions on  $T^4 \times S^1$  with the D5-branes wrapping the full internal space and the D1-branes and KK-momentum on the distinguished  $S^1$ . The notation is best understood by considering the construction of these solutions. One begins with the general solutions of [17] which contain eight parameters: a mass parameter,  $M$ ; spin parameters in two orthogonal planes,  $a_1, a_2$ ; three boost parameters,  $\delta_1, \delta_5, \delta_p$ , which fix the D1-brane, D5-brane and KK-momentum charges, respectively; the radius of the  $S^1$ ,  $R$ ; the volume of the  $T^4$  (which plays no role in the following). The geometry is described by the six-dimensional line element written in Eq. (2.12) of [1], which is parameterized by a time coordinate  $t$ ; a radial coordinate  $r$ ; three angular coordinates  $\theta, \phi, \psi$ ; and the coordinate on the  $S^1$ ,  $y$ .

One then imposes a series of constraints to ensure that the solutions are free of singularities, horizons and closed time-like curves. In particular, one focuses on a low-mass regime,  $M^2 < (a_1 - a_2)^2$ , in which no black holes exist. Then one finds solitonic solutions where an appropriate circle shrinks to zero at the origin and the constraints ensure that this happens smoothly. First,  $M$  and  $R$  can be fixed in terms of the remaining parameters — see Eqs. (3.15) and (3.20) of [1]. Two quantization conditions constrain the remaining parameters in terms of two integers  $m, n$  [1]:

$$\frac{j + j^{-1}}{s + s^{-1}} = m - n, \quad \frac{j - j^{-1}}{s - s^{-1}} = m + n, \quad (8)$$

where  $j = \sqrt{\frac{a_2}{a_1}} \leq 1$  and  $s = \sqrt{\frac{s_1 s_5 s_p}{c_1 c_5 c_p}} \leq 1$ . We are using the notation here that  $c_i \equiv \cosh \delta_i$  and  $s_i \equiv \sinh \delta_i$ . Without loss of generality, one assumes  $a_1 \geq a_2 \geq 0$  which implies  $m > n \geq 0$ . We also note here that the special case  $m = n + 1$  corresponds to supersymmetric solutions.

This leaves a five-parameter family of smooth solitonic solutions. We can think of the independent parameters as the D1-brane and D5-brane charges,  $Q_1, Q_5$ ; the (asymptotic) radius of the  $y$ -circle,  $R$ ; and the two integers,  $m$  and  $n$ , which fix the remaining physical parameters as [1]

$$Q_P = nm \frac{Q_1 Q_5}{R^2}, \quad J_\phi = -m \frac{Q_1 Q_5}{R}, \quad J_\psi = n \frac{Q_1 Q_5}{R}. \quad (9)$$

Of course, depending on the specific application, it may be more appropriate and/or simpler to describe the solutions using a different set of quantities. In our case, when we make explicit calculations of the ergoregion instability, we will fix the parameters  $n, m, a_1, c_1$  and  $c_5$  or  $c_p$ . As we are interested in non-supersymmetric backgrounds, we also impose  $m \geq n + 2$ . To conclude our discussion of notation, we add that the roots of  $g^{rr}$ ,  $r_+$  and  $r_-$ , will also appear in the following but they are determined by  $M$  and the spin parameters — see Eq. (3.2) of [1].

The key ingredient producing the instability in the JMaRT solutions is the existence of an ergoregion. To verify the presence of the ergoregion, one takes as usual the norm of the Killing vector  $V = \partial_t$  and using Eq. (2.12) of [1], calculates

$$g_{\mu\nu} V^\mu V^\nu = -\frac{f - M c_p^2}{\sqrt{\tilde{H}_1 \tilde{H}_5}}, \quad (10)$$

where  $f(r) = r^2 + a_1^2 \sin^2 \theta + a_2^2 \cos^2 \theta > 0$  and  $\tilde{H}_i(r) = f(r) + M s_i^2$ ,  $i = 1, 5$ . It is then clear that  $V = \partial_t$  becomes space-like for  $f(r) < M$  and thus an ergosphere appears at  $f(r) = M$ . An inspection of the metric also allows one to conclude the geometry rotates along  $\phi$ ,  $\psi$  and  $y$  since  $g_{t\phi} \neq 0$ ,  $g_{t\psi} \neq 0$  and  $g_{ty} \neq 0$ . The supersymmetric limit of the JMaRT solitons corresponds to take the limit  $M \rightarrow 0$  and  $\delta_i \rightarrow \infty$ , while keeping the other parameters fixed, including the conserved charges  $Q_i = M s_i c_i$  [1]. So, in the supersymmetric limit the norm becomes  $|V|^2 = -f/\sqrt{\tilde{H}_1 \tilde{H}_5}$ , which is always negative and thus the ergoregion is not present.

Now consider the Klein-Gordon equation for a massless scalar field propagating in the JMaRT geometries,

$$\frac{1}{\sqrt{-g}} \frac{\partial}{\partial x^\mu} \left( \sqrt{-g} g^{\mu\nu} \frac{\partial}{\partial x^\nu} \Psi \right) = 0. \quad (11)$$

Implicitly, we are using the string-frame metric in which case one can think of eq. (11) as the linearized equation of motion for the Ramond-Ramond scalar. As described above, these backgrounds can be thought of as special cases of the general D1-D5-P solutions found earlier [17] and so one may apply separation of variables following [34]. Introducing the following ansatz<sup>5</sup>

$$\Psi = \exp \left[ -i\omega \frac{t}{R} - i\lambda \frac{y}{R} + im_\psi \psi + im_\phi \phi \right] \chi(\theta) h(x), \quad (12)$$

one gets an angular equation

$$\frac{1}{\sin 2\theta} \frac{d}{d\theta} \left( \sin 2\theta \frac{d\chi}{d\theta} \right) + \left[ \Lambda - \frac{m_\psi^2}{\cos^2 \theta} - \frac{m_\phi^2}{\sin^2 \theta} + \frac{\omega^2 - \lambda^2}{R^2} (a_1^2 \sin^2 \theta + a_2^2 \cos^2 \theta) \right] \chi = 0, \quad (13)$$

and a radial equation<sup>6</sup>

$$\begin{aligned} & \frac{1}{r} \frac{d}{dr} \left[ \frac{g(r)}{r} \frac{d}{dr} h \right] - \Lambda h + \left[ \frac{(\omega^2 - \lambda^2)}{R^2} (r^2 + M s_1^2 + M s_5^2) + (\omega c_p + \lambda s_p)^2 \frac{M}{R^2} \right] h \\ & - (r_+^2 - r_-^2) \frac{(\lambda - nm_\psi + mm_\phi)^2}{(r^2 - r_+^2)} h + (r_+^2 - r_-^2) \frac{(\omega \varrho + \lambda \vartheta - nm_\phi + mm_\psi)^2}{(r^2 - r_-^2)} h = 0, \end{aligned} \quad (14)$$

<sup>5</sup> Note that the negative sign for  $\lambda$  corrects a typo found in [1]

<sup>6</sup> Note the factor  $(r_+^2 - r_-^2)$  that appears in the two last terms of the lhs of (14), which are necessary for dimensional consistency, corrects the typo appearing in Eq. (6.4) of [1]

where  $g(r) = (r^2 - r_+^2)(r^2 - r_-^2)$ , and we used  $\sqrt{-g} = r \sin \theta \cos \theta \sqrt{\tilde{H}_1 \tilde{H}_5}$  (this is the determinant of the metric (2.12) of [1]). If we introduce a dimensionless variable

$$x = \frac{r^2 - r_+^2}{r_+^2 - r_-^2}, \quad (15)$$

we can rewrite the radial equation in the form

$$\partial_x [x(x+1)\partial_x h] + \frac{1}{4} \left[ \kappa^2 x + 1 - \nu^2 + \frac{\xi^2}{x+1} - \frac{\zeta^2}{x} \right] h = 0, \quad (16)$$

with

$$\begin{aligned} \kappa^2 &= (\omega^2 - \lambda^2) \frac{r_+^2 - r_-^2}{R^2}, \\ \xi &= \omega \varrho + \lambda \vartheta - m_\phi n + m_\psi m, \\ \zeta &= \lambda - m_\psi n + m_\phi m, \\ \varrho &= \frac{c_1^2 c_5^2 c_p^2 - s_1^2 s_5^2 s_p^2}{s_1 c_1 s_5 c_5}, \\ \vartheta &= \frac{c_1^2 c_5^2 - s_1^2 s_5^2}{s_1 c_1 s_5 c_5} s_p c_p, \end{aligned} \quad (17)$$

and

$$\nu^2 = 1 + \Lambda - \frac{\omega^2 - \lambda^2}{R^2} (r_+^2 + M s_1^2 + M s_5^2) - (\omega c_p + \lambda s_p)^2 \frac{M}{R^2}. \quad (18)$$

The quantities  $\omega$ ,  $\lambda$ ,  $m_\psi$ ,  $m_\phi$  are all dimensionless — the last three being integers. Again, we refer the reader to [1] for a detailed account of the quantities appearing above. The reader should take note that our notation is not in complete accord with that of [1]. That is, to simplify our formulae in the following, we have defined  $\kappa \equiv 1/\sigma$ , the inverse of the quantity  $\sigma$  used there.

Of critical importance in characterizing the solutions of the scalar wave equation is the sign of  $\kappa^2$ . The term  $x\kappa^2$  dominates at large  $x$ , determining the asymptotic behavior of the solution. In this paper we will mainly be interested in outgoing modes so we choose  $\kappa^2$  to be positive. The two remaining possibilities:  $\kappa^2 = 0$  and  $\kappa^2 < 0$ , will be considered in the appendices.

The angular equation (13) (plus regularity requirements) is a Sturm-Liouville problem. We can label the corresponding eigenvalues  $\Lambda$  with an index  $l$ ,  $\Lambda(\omega) = \Lambda_{lm}(\omega)$  and therefore the wavefunctions form a complete set over the integer  $l$ . In the general case, the problem at hand consists of two coupled second order differential equations: given some boundary conditions, one has to compute *simultaneously* both values of  $\omega$  and  $\Lambda$  that satisfy these boundary conditions. However, for vanishing  $a_i^2$  we get the (five-dimensional) flat space result,  $\Lambda = l(l+2)$ , and the associated angular functions are given by Jacobi polynomials. For non-zero, but small  $\frac{\omega^2 - \lambda^2}{R^2} a_i^2$  we have

$$\Lambda = l(l+2) + \mathcal{O} \left( a_i^2 \frac{\omega^2 - \lambda^2}{R^2} \right). \quad (19)$$

The integer  $l$  is constrained to be  $l \geq |m_\psi| + |m_\phi|$ . We will always assume  $a_i^2 \frac{\omega^2 - \lambda^2}{R^2} \ll \max(m_\psi^2, m_\phi^2)$  (with  $i = 1, 2$ ), thus  $\Lambda \simeq l(l+2)$ . Making this assumption implies we may neglect the terms proportional to  $a_i$  in the angular equation, but given the way  $\Lambda$  and  $\omega$  appear in the radial equation, the corrections to  $\Lambda$  may not be negligible when we determine  $\omega$ . To ensure that fixing  $\Lambda = l(l+2)$  is consistent in both the angular and radial equations we must additionally require

$$a_i^2 \ll \max(|r_+^2 + M(s_1^2 + s_5^2)|, M c_p^2), \quad (20)$$

so that the contribution to  $\nu$  from the  $a_i$  dependent corrections of  $\Lambda$  are negligible (see (18)).

Taking the complex conjugate of Eq. (13) we can see that the exact solution to the angular equation has the symmetry

$$\Lambda_{lm}(-\omega^*) = \Lambda_{lm}^*(\omega). \quad (21)$$

With this symmetry, one can also check the following:

$$(\nu^2)^*(\omega, \lambda) = \nu^2(-\omega^*, -\lambda), \quad (22)$$

$$(\xi^2)^*(\omega, \lambda, m_\psi, m_\phi) = \xi^2(-\omega^*, -\lambda, -m_\psi, -m_\phi), \quad (23)$$

$$(\zeta^2)^*(\lambda, m_\psi, m_\phi) = \zeta^2(-\lambda, -m_\psi, -m_\phi). \quad (24)$$

Therefore, from the wave equation (16) it follows that if  $\omega$  is an eigenvalue for given values of  $m_\psi, m_\phi, \lambda$  with eigenfunction  $h$ , then  $-\omega^*$  is an eigenvalue for  $-m_\psi, -m_\phi, -\lambda$  with eigenfunction  $h^*$ . Furthermore, if  $he^{-i\omega t}$  is outgoing unstable, so is  $h^*e^{i\omega^* t}$ . Since the symmetry simultaneously flips all the signs of  $m_\psi, m_\phi, \lambda$ , without loss of generality, we can only fix the sign of one, *e.g.*,  $\mathcal{R}e(\omega) \leq 0$ .

To conclude this section, we point out that the angular equation (13) can be recast in the somewhat more familiar form:

$$\frac{1}{\sin \theta \cos \theta} \frac{d}{d\theta} \left( \sin \theta \cos \theta \frac{d\chi}{d\theta} \right) + \left[ \hat{\Lambda} - \frac{m_\psi^2}{\cos^2 \theta} - \frac{m_\phi^2}{\sin^2 \theta} + \frac{\omega^2 - \lambda^2}{R^2} (a_2^2 - a_1^2) \cos^2 \theta \right] \chi = 0, \quad (25)$$

where

$$\hat{\Lambda} = \Lambda + \frac{\omega^2 - \lambda^2}{R^2} a_1^2. \quad (26)$$

This is just the equation for a five-dimensional scalar spheroidal harmonic [35] which arises, *e.g.*, in the separation of Klein-Gordon equation in the background of a five-dimensional rotating black hole [36].

#### IV. WKB ANALYSIS

We now explicitly show that the JMaRT geometries [1] suffer from an ergoregion instability. As described above, this instability is due to the fact that the geometry has an ergoregion but no horizon. We shall identify modes of the scalar field that are regular at the origin, represent outgoing waves at infinity and grow with time. In this section, we follow the WKB analysis of [27] and show that it applies to the non-supersymmetric JMaRT solutions, with the same qualitative conclusions.

To begin, we want to write the radial wave equation in the form of an effective Schrödinger equation. In order to do so, we first transform to a new ‘wavefunction’  $H$  defined with

$$h(x) = \frac{1}{\sqrt{x(1+x)}} H(x). \quad (27)$$

Inserting this in (16), we get

$$-\partial_x^2 H + U_{\text{eff}} H = 0, \quad (28)$$

where

$$U_{\text{eff}} = -\frac{\kappa^2 x^3 + (1 - \nu^2 + \kappa^2)x^2 + (1 - \nu^2 + \xi^2 - \zeta^2)x + 1 - \zeta^2}{4x^2(1+x)^2}. \quad (29)$$

Now in order to simplify our analysis, we choose:  $\lambda = 0$ ,  $m_\phi = 0$ , and large  $m_\psi$ . With  $\lambda \neq 0$ , the waves see a constant potential at infinity and thus the amplitude of the outgoing waves can be suppressed there. We also consider  $l = m_\psi$  modes, which are expected to be the most unstable. Modes with  $l \gg m_\psi$  must be similar to modes with  $m_\psi = 0$  for some  $l$  and these are not unstable. With these choices, we have

$$\kappa^2 = \omega^2 \frac{r_+^2 - r_-^2}{R^2}, \quad \zeta^2 = n^2 m_\psi^2, \quad \xi^2 = m^2 m_\psi^2 + \omega^2 \varrho^2 + 2\omega \varrho m m_\psi, \quad (30)$$

$$1 - \nu^2 \simeq -m_\psi^2 + \omega^2 \frac{r_+^2 + Ms_1^2 + Ms_5^2 + Mc_p^2}{R^2}. \quad (31)$$

Instead of working directly with the frequency of the wave, it will be convenient to work with the pattern speed along the  $\psi$  direction, which is the angular velocity at which surfaces of constant phase rotate. This velocity is proportional to

$$\Sigma_\psi = \frac{\omega}{m_\psi}, \quad (32)$$

where the proportionality constant  $R^{-1}$  is always positive. It is important to compare the sign of the pattern speed along  $\psi$  with the sign of the angular velocity of the geometry along  $\psi$  defined as usual by<sup>7</sup>

$$\begin{aligned}\Omega_\psi &= -\frac{g_{t\psi}}{g_{\psi\psi}} = -\frac{2Ms_p c_p \cos^2 \theta R/n}{\sqrt{\dot{H}_1 \dot{H}_5} g_{\psi\psi}} \\ &= -\frac{2Q_p \cos^2 \theta \cos^2 \theta R/n}{\sqrt{\dot{H}_1 \dot{H}_5} g_{\psi\psi}} < 0, \quad \forall x > 0,\end{aligned}\quad (33)$$

where  $Q_p = Ms_p c_p$  is the Kaluza-Klein momentum charge. So, when  $\Sigma_\psi$  is negative, the wave is propagating in the same sense as the geometry.

Now it is useful to introduce the polynomial

$$\mathcal{P} = Bx^3 + (A + B)x^2 + (\varrho^2 + A)x, \quad (34)$$

which is positive definite in the range of interest (positive  $x$ ). We also define

$$T = -\frac{U_{\text{eff}}}{m_\psi^2}, \quad A \equiv \frac{r_+^2 + M(s_1^2 + s_5^2 + c_p^2)}{R^2}, \quad B \equiv \frac{r_+^2 - r_-^2}{R^2}. \quad (35)$$

Then, we can write the effective Schrödinger equation (28) as

$$\partial_x^2 H + m_\psi^2 T H = 0, \quad (36)$$

with

$$T = \frac{\mathcal{P}}{4x^2(1+x)^2} \left[ \Sigma_\psi^2 + \frac{2\varrho m x}{\mathcal{P}} \Sigma_\psi - \frac{x^2 - x(m^2 - n^2 - 1) + n^2}{\mathcal{P}} \right], \quad (37)$$

where we have dropped certain small contributions to  $T$ .<sup>8</sup> Now it is straightforward to factorize the potential  $T$  and write it in the form

$$T = \frac{\mathcal{P}}{4x^2(1+x)^2} (\Sigma_\psi - V_+)(\Sigma_\psi - V_-), \quad (38)$$

with

$$V_\pm = -\frac{\varrho m x}{\mathcal{P}} \pm \left[ \left( \frac{\varrho m x}{\mathcal{P}} \right)^2 + \frac{x^2 - x(m^2 - n^2 - 1) + n^2}{\mathcal{P}} \right]^{\frac{1}{2}}. \quad (39)$$

For general  $m, n$  the behavior of the potentials  $V_+$  and  $V_-$  (see Fig. 1) is exactly the same as the one studied in [27], so we do expect an instability to arise, as will be shown below. However, and this is a key point, for the case  $m = n + 1$  which is the supersymmetric case, we have

$$V_+ = -\frac{\varrho m x}{\mathcal{P}} + \left[ \left( \frac{\varrho m x}{\mathcal{P}} \right)^2 + \frac{(x - n)^2}{\mathcal{P}} \right]^{\frac{1}{2}}, \quad m = n + 1, \quad (40)$$

which is always positive. Thus, this WKB analysis indicates that the supersymmetric solutions are stable, as expected.

Hence our radial equation has been reduced to the Schrödinger form (36) with an interesting potential (38), which depends on the pattern speed (32). Now the problem becomes to tune this potential by adjusting  $\Sigma_\psi$  in order that a ‘zero-energy’ solution can be found with the appropriate boundary conditions: regular at the origin and outgoing waves at infinity. Note that in a region where  $\Sigma_\psi$  is above  $V_+$  or below  $V_-$  (allowed regions), the solutions have an oscillatory behavior. In those intervals where  $\Sigma_\psi$  is in between the curves of  $V_+$  and  $V_-$  (forbidden regions), the solutions have a real exponential behavior.

<sup>7</sup> Note that the geometry rotates simultaneously along the  $\psi$ ,  $\phi$  and  $y$  directions. We find  $\Omega_\psi$  using of (2.1), (3.17) and (3.19) of [1].

<sup>8</sup> More precisely, we have dropped a term  $1/(m_\psi^2 \mathcal{P})$ . This remains a very good approximation in the high- $m_\psi$  limit in which we are working. As an example, for  $n = 10$  and  $m_\psi = 10$  the factor that we dropped is  $10^{-4}$  smaller than the last term of (37).



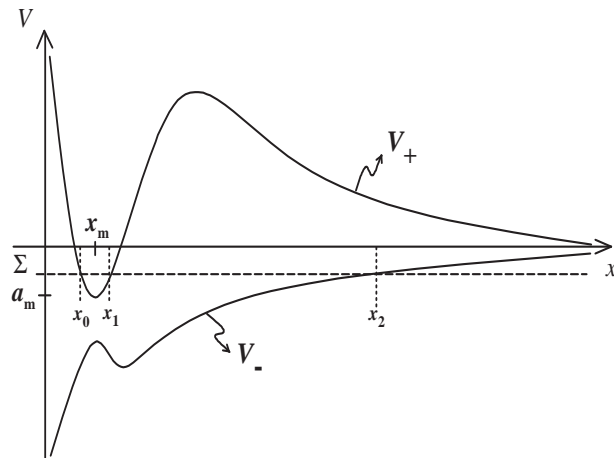


FIG. 1: Qualitative shape of the potentials  $V_+$  and  $V_-$  for the case in which an instability is present. An example of data that yields this kind of potentials is  $(m = 14, n = 10, a_1 = 32, c_1 = 5, c_p = 5)$ . The unstable modes are those whose pattern speed  $\Sigma_\psi$  is negative and approach the minimum of  $V_+$  from above. Thus, they are nearly bound states of the potential well in  $V_+$  that can however tunnel out to infinity through  $V_-$ . Choosing  $\lambda = 0$ , the potentials  $V_+$  and  $V_-$  approach zero as  $x \rightarrow \infty$ , which makes a tunnelling through  $V_-$  easier.

We proceed following [27] and study the scattering of waves in the effective potential constructed above. Consider a wave that comes from infinity with an amplitude  $C_{\text{in}}$ , scatters in the ergoregion and returns to infinity with an amplitude  $C_{\text{out}}$ . In particular, we introduce the scattering amplitude defined as

$$S \equiv \frac{C_{\text{out}}}{C_{\text{in}}}. \quad (41)$$

The presence of a pole in  $S$  (*i.e.*, of a resonance) signals the existence of an instability. Indeed, a pole in  $S$  occurs when  $C_{\text{in}} = 0$  and  $C_{\text{out}} \neq 0$ , and this means that we have finite outgoing radiation for zero incoming radiation. Near the pole frequency  $\omega_p$ , the scattering amplitude can be written to lowest order as [27]

$$S \simeq e^{i2\delta_0} \frac{\omega - \omega_p^*}{\omega - \omega_p}, \quad (42)$$

where  $\delta_0$  is a constant scattering phase shift and  $\omega_p^*$  is the complex conjugate of  $\omega_p$ . Note that this expression guarantees that when the frequency of the wave is real, one has  $S(\omega)[S(\omega)]^* = 1$  as required by energy conservation. Generically, we can write the pole or resonant frequency as

$$\omega_p = \omega_r + i/\tau, \quad (43)$$

where  $\omega_r$  and  $1/\tau$  are, respectively, the real and imaginary parts of  $\omega_p$ . With this convention, a mode with positive  $\tau$  represents an instability, and  $\tau < 0$  represents a damping mode, since the time dependence<sup>9</sup> of the resonant wave is given by  $e^{-i\omega_p t} = e^{-i\omega_r t} e^{t/\tau}$ . We can then write

$$S \simeq e^{i2\delta_0} \frac{\omega - \omega_r + i/\tau}{\omega - \omega_r - i/\tau}. \quad (44)$$

To relate the amplitudes  $C_{\text{in}}$  and  $C_{\text{out}}$  we apply a WKB analysis. As we shall learn later on, the unstable modes are those whose pattern speed  $\Sigma_\psi$  is negative and approaches the minimum of  $V_+$  from above (see Fig. 1). The scattering problem has then four distinct regions, namely: I, the innermost forbidden region ( $0 < x < x_0$ ); II, the allowed region where  $V_+$  is below  $\Sigma_\psi$  ( $x_0 < x < x_1$ ); III, the potential barrier region where  $V_+$  is above  $\Sigma_\psi$  ( $x_1 < x < x_2$ ); and finally

<sup>9</sup> Our conventions differ slightly from those of [27]. There waves carry a time dependence  $e^{i\omega t}$  while we follow [1] which introduces the separation ansatz (12) with a time dependence  $e^{-i\omega t}$ .

the external allowed region where  $\Sigma_\psi$  is below  $V_-$  ( $x_2 < x < \infty$ ). The unstable modes are those that have  $\Sigma_\psi < 0$ . Thus, they are nearly bound states of the potential well in  $V_+$  that can however tunnel out to infinity through  $V_-$ . In region I, the WKB wavefunction that vanishes at the origin  $x = 0$  is

$$H_I \simeq \frac{C_1}{m_\psi^{1/2}|T|^{1/4}} \exp \left[ -m_\psi \int_x^{x_0} \sqrt{|T|} dx \right], \quad (45)$$

where  $C_1$  is an amplitude constant. Then, the usual WKB connection formulae and WKB wavefunctions allow us to relate  $H_I$  with the wavefunctions of the other regions and, in particular, with the incoming and outgoing contributions of the wavefunction  $H_{IV}$  in region IV, which can be written as

$$H_{IV} \simeq \frac{C_6}{m_\psi^{1/2}T^{1/4}} \exp \left[ i m_\psi \int_{x_2}^x \sqrt{T} dx \right] + \frac{C_7}{m_\psi^{1/2}T^{1/4}} \exp \left[ -i m_\psi \int_{x_2}^x \sqrt{T} dx \right]. \quad (46)$$

The WKB analysis yields the relation between the amplitudes  $C_6$ ,  $C_7$  and  $C_1$  (see Appendix A):

$$\begin{aligned} C_1 e^{i\gamma} &= \frac{1}{2} \left[ \left( 2\eta + \frac{1}{2\eta} \right) C_6 + i \left( 2\eta - \frac{1}{2\eta} \right) C_7 \right] \\ C_1 e^{-i\gamma} &= \frac{1}{2} \left[ -i \left( 2\eta - \frac{1}{2\eta} \right) C_6 + \left( 2\eta + \frac{1}{2\eta} \right) C_7 \right], \end{aligned} \quad (47)$$

where

$$\gamma \equiv m_\psi \int_{x_0}^{x_1} \sqrt{T} dx - \frac{\pi}{4}, \quad (48)$$

$$\ln \eta \equiv m_\psi \int_{x_1}^{x_2} \sqrt{|T|} dx. \quad (49)$$

The identification of the ingoing and outgoing contributions in (46) depends on the sign of  $\Sigma_\psi$ . Indeed, one has  $\Psi \propto e^{-i\omega t} H_{IV}(x)$ . If  $\Sigma_\psi$  is negative the term  $C_6 e^{-i(\omega t - \gamma(x))}$  represents the ingoing contribution, while the term  $C_7 e^{-i(\omega t + \gamma(x))}$  describes the outgoing contribution (if  $\Sigma_\psi > 0$ , the terms proportional to  $C_6$  and  $C_7$  in  $H_{IV}(x)$  represent, respectively, the outgoing and ingoing modes). Henceforth we consider the  $\Sigma_\psi < 0$  case (since this will be the unstable case), for which the scattering amplitude can be written as

$$S = \frac{C_7}{C_6} = \frac{i(4\eta^2 - 1)e^{i\gamma} + (4\eta^2 + 1)e^{-i\gamma}}{(4\eta^2 + 1)e^{i\gamma} - i(4\eta^2 - 1)e^{-i\gamma}}. \quad (50)$$

The resonance peaks in the scattering amplitude occur at a frequency  $\omega_N$  for which  $e^{-i\gamma} + i e^{i\gamma} = 0$ , *i.e.*, when  $\gamma(\omega) = \gamma_N$  where

$$\gamma_N(\omega_N) \equiv N\pi + \frac{\pi}{4} \quad (51)$$

with  $N$  being an integer usually referred to as the ‘harmonic’. The easiest way to see that the resonance peaks must be near these (real) frequencies is to note that  $S(\gamma_N) = -i$  while for  $\eta \rightarrow \infty$ , one has  $S(\gamma \neq \gamma_N) = +i$ . So when  $\eta \rightarrow \infty$ , one has generally  $S(\gamma) = +i$ , but when  $\gamma = \gamma_N$  a peak occurs that changes the value of  $S$  from  $+i$  to  $-i$ .

We can now do a Taylor expansion of the functions that appear in  $S$  around  $\gamma = \gamma_N$ . Defining

$$\alpha = \left. \frac{d\gamma}{d\omega} \right|_{\omega=\omega_N} = \frac{d}{d\Sigma_\psi} \left[ \int_{x_0}^{x_1} \sqrt{T} dx \right]_{\Sigma_\psi=\Sigma_{\psi,N}}, \quad (52)$$

the scattering amplitude can be written as

$$S \simeq \frac{-\alpha(\omega - \omega_N) + \frac{1}{4\eta^2} - i \left[ \alpha(\omega - \omega_N) + \frac{1}{4\eta^2} \right]}{-\alpha(\omega - \omega_N) + \frac{1}{4\eta^2} + i \left[ \alpha(\omega - \omega_N) + \frac{1}{4\eta^2} \right]} \quad (53)$$

which, using  $(1+i)/(1-i) = i$ , can be cast in the form

$$S \simeq i \frac{\omega - \omega_N + i \frac{1}{4\eta^2\alpha}}{\omega - \omega_N - i \frac{1}{4\eta^2\alpha}}. \quad (54)$$

This result takes the form (44). Hence the discrete spectrum of resonance frequencies  $\omega_N$  is selected by condition (51). Further comparing (44) with (54), one has that the growth or damping timescale is given by

$$\tau = 4\eta^2\alpha. \quad (55)$$

Now,  $\alpha$  defined in (52) is always positive since as  $\Sigma_\psi$  increases so does  $T$  and  $\gamma$  defined in (48) (the area of the region in between the  $\Sigma_\psi$  line and the  $V_+$  curve, and in between  $\Sigma_\psi$  line and the  $V_-$  curve both increase when  $\Sigma_\psi$  increases). So, we are guaranteed to have a positive  $\tau$  and thus the negative  $\Sigma_\psi$  modes are unstable. If we redo the computations to consider the  $\Sigma_\psi > 0$  case, the only difference is that in (46) the ingoing and outgoing waves are given instead by the terms proportional to  $C_7$  and  $C_6$ , respectively. This changes the scattering amplitude from  $S$  to  $S^{-1}$  and thus  $\tau$  to  $-\tau$  implying that the positive  $\Sigma_\psi$  modes are damped.

Though the resonance frequencies and growth timescales can be computed with numerical methods from (51) and (55), as we shall do in Section VIB, we can still make some further progress analytically by approximating the well of  $V_+$  by a parabola. Near the well, the potential  $V_+$  behaves generally as

$$V_+ \simeq \frac{(x - x_m)^2}{P_m} + a_m, \quad (56)$$

with  $a_m < 0$ . The boundaries  $x_0$  and  $x_1$  are the roots of  $\Sigma_\psi - V_+$ , namely:  $x_0 = x_m - [P_m(\Sigma_\psi - a_m)]^{1/2}$  and  $x_1 = x_m + [P_m(\Sigma_\psi - a_m)]^{1/2}$ . Since  $\sqrt{T}$  vanishes at these boundaries one has

$$\alpha = \int_{x_0}^{x_1} \frac{d\sqrt{T}}{d\Sigma_\psi} dx. \quad (57)$$

Moreover, near the bottom of the well, only  $\Sigma_\psi - V_+$  varies significantly with  $x$ , and we can assume that all the other quantities that appear in the integral of  $\alpha$  are approximately constants given by their value at  $x = x_m$  (the accuracy of this assumption increases as  $\Sigma_\psi$  approaches  $a_m$ ). One then has

$$\alpha \simeq \frac{\Sigma_\psi + \frac{gm x_m}{\mathcal{P}(x_m)}}{\sqrt{\Sigma_\psi - V_-(x_m)}} \frac{\sqrt{\mathcal{P}(x_m)}}{2x_m(1+x_m)} \int_{x_0}^{x_1} [\Sigma_\psi - V_+]^{-\frac{1}{2}} dx, \quad (58)$$

with  $V_+$  given by (56), which yields for  $\alpha$  the value

$$\alpha = \pi \sqrt{P_m} \left[ \Sigma_\psi + \frac{gm x_m}{\mathcal{P}(x_m)} \right] [\Sigma_\psi - V_-(x_m)]^{-1/2} \frac{\sqrt{\mathcal{P}(x_m)}}{2x_m(1+x_m)}. \quad (59)$$

Let us illustrate the use of the WKB method we have described in this section to compute the instability parameters in a particular configuration. Take,

$$m = 14; n = 10; a_1 = 32; c_1 = 5; c_p = 5; \quad (60)$$

$$\lambda = m_\phi = 0; l = m_\psi = 10. \quad (61)$$

By approximating the well in  $V_+$  by a parabola, as in (56), we get

$$a_m = -0.17894; x_m = 9.1537; P_m = 2759.4. \quad (62)$$

The resonant frequencies are those that satisfy condition (51) with  $\gamma(\omega)$  given by (48). For the fundamental harmonic ( $N = 0$ ), we get

$$\Sigma_\psi = -0.173. \quad (63)$$

The growth timescale of the instability is given by (55) with  $\eta(\omega_N)$  given by (49). Again, for  $N = 0$  we get

$$\tau \sim 10^{47}. \quad (64)$$

Independently of the parameters of the geometry, we note that as  $m_\psi$  grows,  $\Sigma_\psi$  approaches  $a_m$ , the value of the  $V_+$  at its minimum. For the particular geometry parameters described in (60) we have (for  $\lambda = m_\phi = 0$ ):

$$\begin{aligned} m_\psi = 10 : \Sigma_\psi &= -0.173, \\ m_\psi = 20 : \Sigma_\psi &= -0.176, \\ m_\psi = 40 : \Sigma_\psi &= -0.177. \end{aligned} \tag{65}$$

This feature can be proved analytically, as was done in [27].

Let us verify consistency of our results. We have assumed that  $a_i^2 \frac{\omega^2 - \lambda^2}{R^2} \ll 1$  in order to do the approximation  $\Lambda \simeq l(l+2)$ . Now, for the cases we listed above one has  $a_i^2 \frac{\omega^2 - \lambda^2}{R^2} \sim 10^{-2}$ , which is inside the range of validity for our approximations. A different combination of parameters yields a different instability timescale, and resonant frequency, so there are geometries more unstable than others. The following refers to the fundamental harmonic, and are computed within the parabolic approximation. We work with the following parameters:

$$c_1 = 5; c_p = 5; \lambda = m_\phi = 0; l = m_\psi = 10. \tag{66}$$

For the fundamental harmonic we then get

$$m = 1400; n = 10; a_1 = 32; \Sigma_\psi = -0.40502, \tau \sim 3 \times 10^{82} \tag{67}$$

$$m = 12; n = 10; a_1 = 32; \Sigma_\psi = -0.104, \tau \sim 3 \times 10^{52} \tag{68}$$

$$m = 14; n = 10; a_1 = 3200; \Sigma_\psi = -0.1728, \tau \sim 3 \times 10^{48} \tag{69}$$

$$m = 3; n = 1; a_1 = 32; \Sigma_\psi = -0.0148, \tau \sim 3 \times 1.7 \times 10^{44} \tag{70}$$

It also evident that the instability is much stronger for small values of  $m_\psi$ , where the WKB is expected to break down.

To conclude this section, let us consider the regime of validity of the WKB approximation with more detail. A standard analysis of Eq. (28) suggests the WKB approximation is valid for  $|\partial_x U_{\text{eff}}| \ll |U_{\text{eff}}|^2$ , which can be rewritten as  $|\partial_x T/T^2(x)| \ll m_\psi^2$ . So, for large  $m_\psi$ , the WKB approximation seems to be valid quite generally. However, we must sound a note of caution. As we already remarked, Eq. (65) shows that as  $m_\psi$  grows,  $\Sigma_\psi$  approaches  $a_m$ , the value of the  $V_+$  at its minimum — this can be proved analytically [27]. So when  $m_\psi$  becomes very large, the two turning points are very close and the WKB analysis breaks down because  $T(x) \rightarrow 0$ . So we conclude that the WKB approximation used in this section should be valid in a regime with large  $m_\psi$ , but not exceedingly large. In any event, it is clear that the instability is strongest for small values of  $m_\psi$ , when the WKB analysis is certainly not valid. So, in the next two sections we will compute the features of the instability using complementary methods valid for small values of  $m_\psi$ . We will also find remarkable agreement between all three approaches.

## V. MATCHED ASYMPTOTIC EXPANSION ANALYSIS

The WKB analysis described in the last section appears to be strongest when describing solutions for which  $\kappa^{-1} \sim \zeta, \xi$ , but in general this corresponds to solutions with high angular momentum. In the sense that the timescale of the instability due to these modes is largest, they are the least unstable. Conversely, the matched asymptotic expansion that we use in this section becomes valid when  $\kappa^{-1} > \zeta, \xi$ , they are the dominant decay modes. As an additional bonus, the eigenvalues are determined explicitly through algebraic constraints. Having both approximations at our disposal allows us to accurately calculate the eigenvalues for most of the allowed parameters.

We follow a matching procedure introduced in [37], which has previously been used for studying scalar fields in three-charge geometries by Giusto, Mathur and Saxena [20], in the JMaRT backgrounds [1] and also in [24, 31–33, 38]. The space is divided into two parts: a near-region,  $x \ll \beta$ , and a far-region,  $x \gg \alpha$ , such that  $\alpha \ll \beta$ . The radial equation is then solved approximately and the appropriate boundary conditions applied in each of the two regions. Finally, we match the near-region and the far-region solutions in the area for which they are both valid,  $\alpha \ll r \ll \beta$ . This gives a set of constraints, the solution of which gives the eigenvalues. Performing this analysis for the radial equation (16), we shall see that the only solutions which are regular at the origin and purely outgoing at infinity are finite as  $x \rightarrow \infty$ , and lead to instabilities. Except when otherwise stated, the analysis in this section will hold for general values of  $m_\psi, m_\phi$  and  $\lambda$ .

### A. The near region solution

In the near-region,  $\kappa^2 x \ll |1 - \nu^2|$ , one can neglect the  $\kappa^2 x$  term, and the radial equation (16) is approximated by

$$x(1+x)\partial_x^2 h + (1+2x)\partial_x h + \frac{1}{4} \left[ 1 - \nu^2 + \frac{\xi^2}{x+1} - \frac{\zeta^2}{x} \right] h = 0. \quad (71)$$

With the definition  $h = x^{|\zeta|/2}(1+x)^{\xi/2} w$ , the near-region radial equation becomes a standard hypergeometric equation [39] of the form

$$x(1+x)\partial_x^2 w + [c + (a+b+1)x]\partial_x w + ab w = 0, \quad (72)$$

where

$$a = \frac{1}{2}(1 + |\zeta| + \xi + \nu), \quad b = \frac{1}{2}(1 + |\zeta| + \xi - \nu), \quad c = 1 + |\zeta|. \quad (73)$$

The full solution to the above is given in terms of hypergeometric functions as  $w = A F(a, b, c, -x) + B x^{1-c} F(a - c + 1, b - c + 1, 2 - c, -x)$ , which allows us finally to write the solution of the radial equation in the near region as

$$h = A x^{|\zeta|/2} (1+x)^{\xi/2} F(a, b, c, -x) + B x^{-|\zeta|/2} (1+x)^{\xi/2} F(a - c + 1, b - c + 1, 2 - c, -x). \quad (74)$$

At this point we impose the first boundary condition: the solution must be regular at  $x = 0$  since the geometry is smooth at the origin of the ‘‘core’’. The term proportional to  $x^{-|\zeta|/2}$  diverges at  $x = 0$  and must be discarded, *i.e.*, its coefficient,  $B$ , must be set to zero.

To perform the matching we need to know the large  $x$  behavior of the regular near-region solution. To this end, one uses the  $x \rightarrow 1/x$  transformation law for the hypergeometric function [39]

$$F(a, b, c, -x) = \frac{\Gamma(c)\Gamma(b-a)}{\Gamma(b)\Gamma(c-a)} x^{-a} F(a, 1-c+a, 1-b+a, -1/x) + \frac{\Gamma(c)\Gamma(a-b)}{\Gamma(a)\Gamma(c-b)} x^{-b} F(b, 1-c+b, 1-a+b, -1/x), \quad (75)$$

and the property  $F(a, b, c, 0) = 1$ . Note that this expression for the transformation is only valid when  $a - b = \nu$  is non-integer. This is an assumption we will continue to make throughout this section. In the end, we shall derive a condition determining the allowed eigenvalues that will not be dependent upon this assumption and therefore we may extend our results to integer values of  $\nu$  by continuity.

The large  $x$  behavior of the near-region solution is then given by

$$h \sim A \Gamma(1 + |\zeta|) \left[ \frac{\Gamma(-\nu)}{\Gamma[\frac{1}{2}(1 + |\zeta| + \xi - \nu)] \Gamma[\frac{1}{2}(1 + |\zeta| - \xi - \nu)]} x^{-\frac{\nu+1}{2}} + \frac{\Gamma(\nu)}{\Gamma[\frac{1}{2}(1 + |\zeta| + \xi + \nu)] \Gamma[\frac{1}{2}(1 + |\zeta| - \xi + \nu)]} x^{\frac{\nu-1}{2}} \right]. \quad (76)$$

### B. The far region solution

In the far-region,  $\kappa x^2 \gg \max\{\xi^2 - 1, \zeta^2\}$ , the terms  $\xi^2/(x+1)$  and  $\zeta^2/x$  can be neglected, and the radial equation can be approximated by

$$\partial_x^2(xh) + \left[ \frac{\kappa^2}{4x} - \frac{\nu^2 - 1}{4x^2} \right] (xh) = 0. \quad (77)$$

The most general solution of this equation when  $\nu$  is non-integer is a linear combination of Bessel functions of the first kind [39],

$$h = x^{-1/2} [C J_\nu(\kappa\sqrt{x}) + D J_{-\nu}(\kappa\sqrt{x})]. \quad (78)$$

This form does not lend itself easily to application of the boundary conditions. Instead, for large  $\kappa\sqrt{x}$ , the solution may be expanded as [39]

$$h \sim \frac{x^{-3/4}}{\sqrt{2\pi\kappa}} \left[ e^{i\kappa\sqrt{x}} e^{-i\frac{\pi}{4}} (C e^{-i\frac{\pi\nu}{2}} + D e^{i\frac{\pi\nu}{2}}) + e^{-i\kappa\sqrt{x}} e^{i\frac{\pi}{4}} (C e^{i\frac{\pi\nu}{2}} + D e^{-i\frac{\pi\nu}{2}}) \right]. \quad (79)$$

As in the WKB analysis, we assume that the real part of  $\omega$  is negative, and therefore the positive and negative sign exponentials give, respectively, ingoing and outgoing waves. We require that there be purely outgoing waves at infinity and so impose the constraint that the coefficient of the positive exponential vanishes, yielding

$$C = -D e^{i\pi\nu}. \quad (80)$$

When  $\omega$  becomes complex, so too does  $\kappa$ . Since the sign of the real part of  $\omega$  is negative, the definition of  $\kappa$  (17) implies that its imaginary part has a sign opposite that of the imaginary part of  $\omega$ . Therefore, requiring additionally that the solution be finite as  $x \rightarrow \infty$  implies that the imaginary part of  $\omega$  must be positive. This is precisely the sign for the imaginary part of the frequency that leads to instabilities. Thus we see that simply requiring the solutions with complex frequency be finite at infinity automatically guarantees they lead to instabilities.

Now, to do the matching in the overlapping region, we will need to know how the far-region solution behaves for small values of  $x$ . More specifically, for small  $\kappa\sqrt{x}$ , and considering only the dominant terms, the solution behaves as [39]

$$h \sim D \left[ \frac{(2/\kappa)^{-\nu}}{\Gamma(1+\nu)} x^{\frac{\nu-1}{2}} - e^{i\pi\nu} \frac{(2/\kappa)^\nu}{\Gamma(1-\nu)} x^{-\frac{\nu+1}{2}} \right]. \quad (81)$$

### C. Matching conditions: Selection of frequencies

We will now determine the frequencies that can appear when the geometry is perturbed by a scalar field. The frequency spectrum is not arbitrary: only those values that satisfy the matching conditions between the near-region and the far-region are allowed. We shall see that there are two solutions of the matching equations, yet only one will lead to instabilities.

Matching the powers of  $x$  between the near (76) and far-region solutions (81), and taking a ratio to eliminate the amplitudes  $A$  and  $D$ , yields

$$-e^{i\pi\nu} (\kappa/2)^{2\nu} \frac{\Gamma(1-\nu)}{\Gamma(1+\nu)} = \frac{\Gamma(\nu)}{\Gamma(-\nu)} \frac{\Gamma(\frac{1}{2}(1-\nu+|\zeta|+\xi))}{\Gamma(\frac{1}{2}(1+\nu+|\zeta|+\xi))} \frac{\Gamma(\frac{1}{2}(1-\nu+|\zeta|-\xi))}{\Gamma(\frac{1}{2}(1+\nu+|\zeta|-\xi))}. \quad (82)$$

The problem of finding the outgoing modes thus boils down to solving the single transcendental equation (82); we will do so by iteration. Note that the  $\kappa$  dependence on the left hand side means that it is suppressed. For the equation to hold, a similar suppression must also occur on the right hand side. This is only possible if one of the gamma functions in the denominator of the right side is large. Since the gamma function diverges when its argument is a non-positive integer, we take as a first iteration the choice

$$\nu + |\zeta| - \xi = -(2N + 1), \quad (83)$$

where the non-negative integer  $N$  will again be referred to as the harmonic. Note that we could also have chosen the above relation, but with the opposite sign for  $\xi$ . While this does indeed lead to a solution, one finds that the imaginary part of the frequency is always negative, *i.e.*, the modes are exponentially damped in time.

This first estimate is obviously not the end of the story as it would cause the right side to completely vanish. To go beyond this approximation, we rewrite Eq. (82) in terms of  $N$ , then perturb  $N \rightarrow N + \delta N$ , where  $\delta N \ll N$ . This deformation appears at leading order only for the  $\Gamma$  function in the denominator on the right hand side that diverges, it may be neglected in all other factors. More concretely, to extract  $\delta N$  from the  $\Gamma$  function we use  $\Gamma(z)\Gamma(1-z) = \pi/\sin(\pi z)$ , and sine function identities to obtain the expansion

$$\Gamma(-N - \delta N) \approx - [(-1)^N N! \delta N]^{-1}. \quad (84)$$

Substituting this into (82), and using a number of  $\Gamma$  function identities, we solve for the imaginary part of the first correction

$$\mathcal{I}m(\delta N) = \pi \frac{(\kappa/2)^{2\nu}}{\Gamma^2(\nu)} [\nu]_N [\nu]_{N+|\zeta|}, \quad (85)$$

where  $[a]_n = \prod_{i=1}^n (1 + a/i)$ . Since  $N$  is  $\mathcal{O}(1)$  and  $\delta N \sim \kappa^{2\nu}$ , we see that we may stop after the first iteration. As a function of  $\nu$ , this can have a single maximum near  $\nu \sim \kappa$ . In general we will have  $\kappa \ll 1$  and  $\nu \sim 1 + l$ , so will always be in a region where this is a monotonically decreasing function of  $\nu$ . For fixed  $\nu$ , the last two factors make this an increasing function of  $N$  and  $|\zeta|$ , but the general behavior will be dominated by the effects of changing  $\nu$ .

The equation (83) uniquely determining  $\omega$  can be exactly solved

$$(\varepsilon + \varrho^2)\omega = -\left(\lambda \frac{s_p c_p M}{R^2} + \varrho c\right) + \sqrt{\left(\lambda \frac{s_p c_p M}{R^2} + \varrho c\right)^2 - (\varepsilon + \varrho^2)(c^2 - \nu_0^2)}, \quad (86)$$

where

$$\varepsilon \equiv \frac{1}{R^2}(r_+^2 + M(s_1^2 + s_5^2 + c_p^2)), \quad c \equiv \xi_0 - |\zeta| - (2N + 1), \quad (87)$$

and a variable with a subscripted 0 means we have set  $\omega = 0$ . Note that as long as  $m \geq n + 2$ , we have  $\varepsilon/\varrho^2 \ll 1$  and both quantities are positive. When  $m \rightarrow n + 1$ , though,  $\varepsilon \rightarrow -\infty$  (since  $M \rightarrow 0$ ,  $r_+^2 \rightarrow -\infty$  and  $R^2$  stays finite), ensuring that there can be no instability for the supersymmetric solutions. This extends to arbitrary modes the conclusion from the discussion associated to equation (40) for modes with  $m_\phi = \lambda = 0$ .

When evaluated on a solution,  $\nu$  is given by  $\nu = \omega\varrho + c$ . Since we are interested in solutions for which  $\omega$  is negative, this means  $c > 0$ . Then, requiring that  $\omega$  be negative and real, gives three more conditions. The first ensures that the result is real while the second requires that the first term of (86) is negative. Finally, the condition that appears to be the most difficult to satisfy ensures the contribution from the square root does not make the total result positive, *i.e.*,

$$c^2 - \nu_0^2 > 0. \quad (88)$$

When  $\lambda \neq 0$ , these conditions must also be supplemented by the requirement that  $\omega^2 - \lambda^2 > 0$ , which ensures the asymptotic behavior of the solution is correct. With these satisfied, we may determine the effect of the correction.

The imaginary contribution to  $N$  is taken as resulting from a small imaginary correction to  $\omega$ . Then, the two are related through

$$\begin{aligned} \delta N &= \frac{\delta\omega}{2} \frac{d}{d\omega} (\xi - \omega) \Big|_N \\ &= \frac{\delta\omega}{2\nu} [(\varrho^2 + \varepsilon)\omega + (\lambda s_p c_p M/R^2 + \varrho c)] \\ &= \frac{\delta\omega}{2\nu} \sqrt{\left(\lambda \frac{s_p c_p M}{R^2} + \varrho c\right)^2 - (\varepsilon + \varrho^2)(c^2 - \nu_0^2)}. \end{aligned} \quad (89)$$

In the final line we have used the solution (86) to show that the sign of  $\delta N$  determines the sign of the correction to  $\omega$ . Since  $\mathcal{I}m(\delta N)$  is always positive when evaluated on the solution of (83), the corresponding imaginary part of  $\omega$  is positive.

To summarize, whenever the constraints, in particular (88), are satisfied there is a corresponding outgoing mode of the scalar field equation. Further, the imaginary part of the frequency of this mode is guaranteed to be positive, indicating that it leads to an instability. The timescale for the instability generated by the mode is a monotonically increasing function of  $\nu$ , which is given by

$$(\varepsilon + \varrho^2)\nu = \varepsilon c - \lambda \varrho s_p c_p \frac{M}{R^2} + \sqrt{\left(\varepsilon c - \lambda \varrho s_p c_p \frac{M}{R^2}\right)^2 + (\varepsilon + \varrho^2)(2c\varrho\lambda s_p c_p \frac{M}{R^2} + \nu_0^2\varrho^2 - \varepsilon c^2)}. \quad (90)$$

A similar argument, based on the solution of equation (83), but with the opposite sign for  $\xi$  would lead to a set of outgoing modes with an amplitude that decays in time.

As an example, consider the particular background geometry and scalar field solution described by

$$\begin{aligned} m &= 5; \quad n = 1; \quad a_1 = 19.1; \quad c_1 = 5; \quad c_p = 1.05; \\ \lambda &= m_\phi = 0; \quad l = m_\psi = 2. \end{aligned} \quad (91)$$

The first two iterations with  $N = 0$  gives

$$\begin{aligned} \omega &= -2.8717, \\ \tau^{-1} = \mathcal{I}m(\delta\omega) &= 4.42 \times 10^{-11}, \end{aligned} \quad (92)$$

The results obtained here are consistent with the WKB analysis of the last section, *i.e.*, there are outgoing modes that rotate in the same sense as the background geometry whose amplitude grows exponentially in time. What we have gained is an explicit set of relations that allows the unstable mode frequencies to be calculated. In particular, one can now make definite statements about the relative timescales for unstable modes just by looking at equation (90). We leave the precise details of this to Appendix C and just give the results here. The most unstable modes are those which minimize  $\nu$ . Since  $\varepsilon \ll \varrho^2$  this generally means that the modes which maximize  $c$  or minimize  $\nu_0$  will be the most unstable. In general this means we should consider the lowest possible  $l$  for which the constraints can be satisfied when setting  $m_\psi = l$ ,  $m_\phi = 0$  and  $N = 0$ .

A second benefit of this analysis is an improvement in accuracy for the most unstable modes. For comparison, performing the WKB analysis and not neglecting any terms in the potentials or approximating the bottom of the well with a parabola gives  $\omega = -3.129 + 4.00 \times 10^{-10}i$ . From the full numerical solution we have  $\omega = 2.8718 + 4.46 \times 10^{-11}i$ . For values of  $\omega$  in this range we have  $\kappa^{-2} \sim 1900$ , so we are well within the range for which we should trust this solution. As  $\kappa^{-1}$  approaches  $\max(|\zeta|, \xi)$ , this analysis begins to break down, but it appears that the WKB approach becomes increasingly accurate. In the next section we will present a more detailed list of eigenvalues corresponding to instabilities and discuss the results.

## VI. NUMERICAL RESULTS

We will now solve the radial equation (16) numerically to extract the instability. We begin with an exposition of the numerical algorithm. The only approximation used in this section concerns the angular eigenvalue  $\Lambda$ , that we shall assume to be well described by (19). At the end of the calculation we always make sure the result fits the regime of validity of this approximation. Note, however, solutions can still be found even when outside this range. The easiest way to do this is by treating  $\Lambda$  and  $\omega$  respectively as eigenvalues of the angular and radial equations. The coupled system may then be solved by first assuming the approximation to hold and solving the radial equation for  $\omega$ , this is then fed into the angular equation to obtain an improved value of  $\Lambda$ . This process may be iterated until the desired level of convergence is achieved.

### A. Numerical procedure

The method of finding solutions numerically is very much like performing the matched expansions. We use Eqs. (74) and (78) to fix the initial conditions for two integrations of the exact radial equation. Since the equation of motion is linear, we may immediately match the two solutions at a point in the interior region by rescaling. This leaves two more conditions to be satisfied, that matching of the derivatives of the real and imaginary parts. Fixing all other parameters, we vary the real and imaginary parts of  $\omega$  to satisfy these conditions.

Given the small size of the expected imaginary part, it is most straightforward to use a package like Mathematica [40] with its software based arbitrary precision, to perform the calculations. Satisfying the matching conditions can be done by treating the difference in derivatives at the interior point as a complex valued function of  $\omega$ . A root may then be searched for using the built-in function `FindRoot` which, for a function without explicit derivatives, looks for the solution by constructing secants.

Since the imaginary part is expected to be far smaller than the real, gradients of the matching function in the imaginary  $\omega$  direction will be large only when very near a solution, but negligible elsewhere. The initial guesses at the solution are therefore very important for ensuring that iterations converge to a solution. It was found empirically that solutions could consistently be found by choosing to start the search in a region around the real value of  $\omega$  for which the inner solution vanishes at the matching point. Small changes in the imaginary part of  $\omega$  near this point appear to be sufficient to bring about convergence. In Fig. 2 we show an example solution obtained in this manner. The solid line is the full numeric solution, with the integration starting at small  $x$  in red to the left of the black dot and that starting at large  $x$  on the right in blue. The dashed lines are the near (74) and far (78) approximations used to set the initial conditions for integrating the exact radial equation. The fact that the imaginary part of  $\omega$  is in general very small raises non-trivial problems, related to the number of digits of precision used and the exact way in which boundary conditions are applied. A discussion of these aspects is deferred to Appendix B.



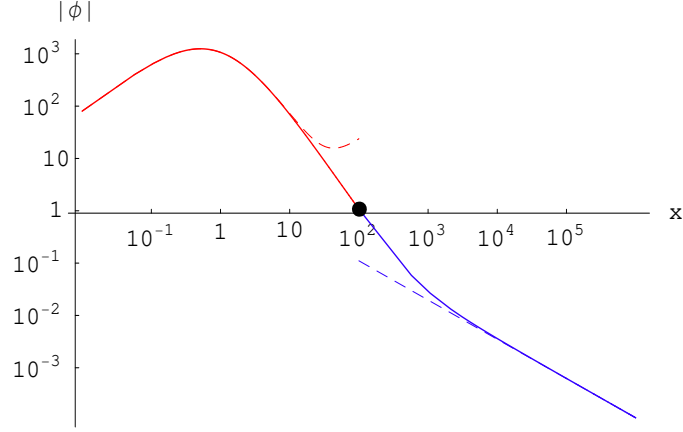


FIG. 2: An example solution showing vanishing as both  $x \rightarrow 0$  and  $x \rightarrow \infty$ .

### B. Numerical results

Our numerical results are summarized in Fig. 3 and Table I. In Fig. 3 on the left we present the numerical solutions obtained for

$$m = 5, n = 1, c_1 = 1.1, c_5 = 1.52, a_1 = 262.7, \lambda = m_\psi = 0. \quad (93)$$

where we consider only the lowest harmonic,  $N = 0$ , but vary  $l = m_\psi$ . At  $l = 1$ ,  $\kappa^{-1} \sim 40$  indicating the matched solution is valid, as  $l$  grows so do  $\xi, \zeta$  while  $\kappa^{-1}$  shrinks, meaning the approximation should soon break down. At  $l = 5$ ,  $\kappa^{-2} \sim 10$  and the approximation is becoming no longer valid. Finally, when  $l = 13$ ,  $\kappa^{-2} \sim 1$  and differences between the matched and numerically determined eigenvalues are starting to become apparent. In Fig. 3 on the right, we use the same parameters as before, but now fix  $l = m_\psi = 4$  and vary the harmonic from  $N = 0$  up to 4. Increasing  $N$  leads to smaller values of  $\omega$  and therefore smaller values of  $\kappa$ , so that the matched solutions are valid throughout. It should also be noted that if the approximation  $a_1^2 \omega^2 / R^2 \ll m_\psi^2$  is valid for a given  $m_\psi$ , then it should be valid for all  $m_\psi$ . This is because  $\omega$  scales with  $m_\psi$ , as we observed within the WKB approximation.

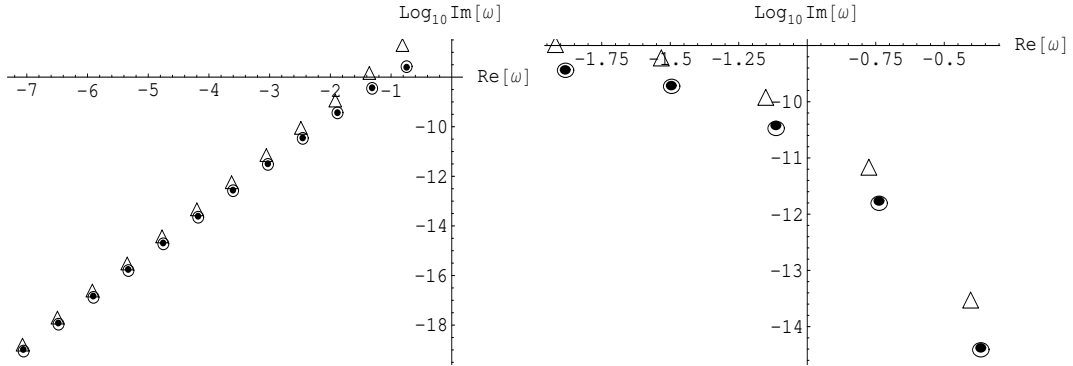


FIG. 3: On the left we choose the lowest harmonic and vary  $l = m_\psi$  from 2 to 13 from upper right to lower left. The solid circles represent the numeric solutions, while the triangles are the results of the WKB analysis and the unfilled circles correspond to the matched expansion. On the right we fix  $l = m_\psi = 4$  and vary the harmonic from 0 to 4 from upper left to lower right.

In Table I we present and compare the numerical results with those obtained through the approximate analytical approaches. The values labeled as  $\text{WKB}_{\text{NUM}}$  (numerical WKB) stand for values obtained using the full WKB approximation, formulae (48), (49), (51) and (55), which have been handled numerically. The values obtained using the parabolic approximation, formulae (56)-(59), for the potential are denoted by  $\text{WKB}_{\text{AN}}$ .

$m_\psi$	Numeric	WKB <sub>NUM</sub>	WKB <sub>AN</sub>	Matching
1	$-0.184 + 3.83 \times 10^{-8}i$	—	—	$-0.184 + 3.83 \times 10^{-8}i$
2	$-0.744 + 2.51 \times 10^{-8}i$	$-0.812 + 1.61 \times 10^{-7}i$	$-0.826 + 1.89 \times 10^{-7}i$	$-0.744 + 2.64 \times 10^{-8}i$
3	$-1.312 + 3.73 \times 10^{-9}i$	$-1.359 + 1.20 \times 10^{-8}i$	$-1.371 + 1.48 \times 10^{-8}i$	$-1.312 + 3.53 \times 10^{-9}i$
4	$-1.883 + 3.69 \times 10^{-10}i$	$-1.919 + 9.33 \times 10^{-10}i$	$-1.932 + 1.17 \times 10^{-9}i$	$-1.882 + 3.63 \times 10^{-10}i$
5	$-2.456 + 3.55 \times 10^{-11}i$	$-2.486 + 7.37 \times 10^{-11}i$	$-2.499 + 9.39 \times 10^{-11}i$	$-2.454 + 3.39 \times 10^{-11}i$
6	$-3.030 + 3.22 \times 10^{-12}i$	$-3.055 + 5.89 \times 10^{-12}i$	$-3.072 + 7.62 \times 10^{-12}i$	$-3.028 + 3.02 \times 10^{-12}i$
7	$-3.605 + 2.77 \times 10^{-13}i$	$-3.626 + 4.73 \times 10^{-13}i$	$-3.647 + 6.23 \times 10^{-13}i$	$-3.602 + 2.63 \times 10^{-13}i$
8	$-4.180 + 2.47 \times 10^{-14}i$	$-4.199 + 3.82 \times 10^{-14}i$	$-4.216 + 4.88 \times 10^{-14}i$	$-4.176 + 2.24 \times 10^{-14}i$
9	$-4.755 + 2.05 \times 10^{-15}i$	$-4.772 + 3.09 \times 10^{-15}i$	$-4.794 + 4.03 \times 10^{-15}i$	$-4.751 + 1.89 \times 10^{-15}i$
10	$-5.331 + 1.76 \times 10^{-16}i$	$-5.346 + 2.51 \times 10^{-16}i$	$-5.369 + 3.26 \times 10^{-16}i$	$-5.326 + 1.58 \times 10^{-16}i$
11	$-5.907 + 1.49 \times 10^{-17}i$	$-5.921 + 2.03 \times 10^{-17}i$	$-5.947 + 2.65 \times 10^{-17}i$	$-5.902 + 1.32 \times 10^{-17}i$
12	$-6.483 + 1.22 \times 10^{-18}i$	$-6.496 + 1.65 \times 10^{-18}i$	$-6.516 + 2.07 \times 10^{-18}i$	$-6.477 + 1.09 \times 10^{-18}i$
13	$-7.059 + 1.04 \times 10^{-19}i$	$-7.071 + 1.34 \times 10^{-19}i$	$-7.102 + 1.81 \times 10^{-19}i$	$-7.053 + 8.97 \times 10^{-20}i$

TABLE I: Some numerical values of the instability for a geometry with  $m = 5$ ,  $n = 1$ ,  $c_1 = 1.10$ ,  $c_5 = 1.52$ ,  $a_1 = 262.7$ ,  $\lambda = m_\psi = 0$  and  $l = m_\psi$ . In the second column, we have the results of the full numerical analysis; in the third column, WKB<sub>NUM</sub> (numerical WKB) stands for values obtained using the full WKB approximation, formulae (48), (49), (51) and (55); and in the fourth column, labelled as WKB<sub>AN</sub>, the values obtained using the parabolic approximation for the potential, formulae (56)-(59), are given. In the final column, we present the results of the matching procedure (83),(85). Notice the close agreement between all the different methods. For  $m_\psi = l = 1$  and for these particular values of the parameters, the WKB analysis, as done here, breaks down. Indeed, for  $m_\psi = 1$ , the potential  $V_+$  has no minimum.

Notice first that all the different approaches yield consistent and in fact very similar results: they are all rather accurate in their own regime of validity. As predicted by the analytic approaches, and verified numerically, the real part of the frequency scales with  $m_\psi$ , whereas the logarithm of the imaginary part scales with  $m_\psi$ , *e.g.*, see Eq. (49). Thus the instability timescale increases rapidly as a function of  $m_\psi$ .

## VII. DISCUSSION

In this paper, we have shown that the non-supersymmetric JMaRT solitons [1] are classically unstable. The relevant instabilities are quite generic to spacetimes which have an ergoregion but are horizon-free [26]. However, as noted in Section II B, the general proof does not strictly apply to the JMaRT solutions since the latter support nonradiative negative energy modes as shown in Appendix D. Hence we have explicitly shown that the ergoregion instabilities are active in the JMaRT geometries using three different approaches, which in the end show a remarkable agreement — see Fig. 3 and Table I. Perhaps the most physically intuitive method is the WKB analysis carried on in Sec. IV. This approach allows us to clearly identify the nature and physical properties of the instability. However, this analysis is only expected to be valid for large angular momentum quantum numbers, *i.e.*,  $m_\psi \gg 0$ , which is not where the instability is strongest. The more unstable modes were studied using the matched asymptotic expansion method [37] in Sec. V. As a final consistency check of these analytical results, we made a numerical analysis of the wave equation in Sec. VI.

In passing we note by considering orbifolds, the JMaRT solutions were extended to a six-parameter family which includes a third integer  $k$  characterizing the orbifold group  $\mathbb{Z}_k$  [1]. Of course, it is straightforward to adapt our instability analysis so that the modes respect this orbifold symmetry in the covering space and so one concludes that the ergoregion instability arises in these orbifold geometries as well.

Let us now summarize some of the features of the ergoregion instability found for the JMaRT solutions:

(i) The general shape of the WKB potentials  $V_\pm$  are sketched in Fig. 1 for the case in which an instability is present. The key point is that when the ergoregion is present the bottom of the potential well in  $V_+$  reaches negative values. The unstable modes are those whose pattern speed  $\Sigma_\psi$  is negative and approaches the minimum of  $V_+$  from above (see Fig. 1). Thus, they are nearly bound states of the potential well in  $V_+$  that can however tunnel out to infinity through  $V_-$ .

(ii) The fact that the unstable modes are those with negative phase velocity,  $\Sigma_\psi < 0$ , has a clear physical interpretation. As in the discussion of Eqs. (32) and (33), modes with  $\Sigma_\psi < 0$  are those that propagate in the same sense as geometry's rotation  $\Omega_\psi$ . Therefore at infinity these modes carry positive angular momentum (same sense as  $\Omega_\psi$ ), as well as positive

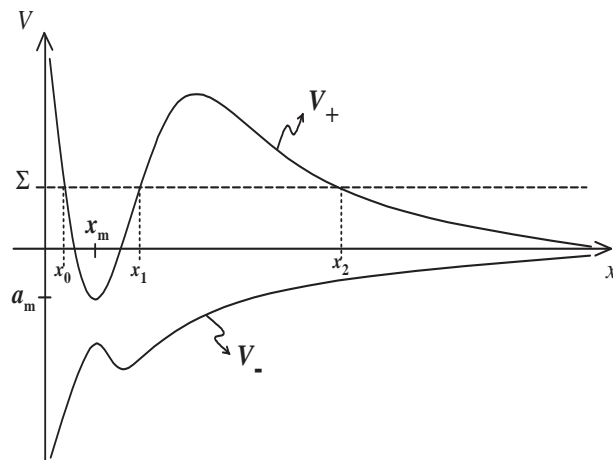


FIG. 4: Damped modes are those that have positive  $\Sigma_\psi$ .

energy. Hence by conservation of energy and angular momentum, with the onset of the ergoregion instability, the JMaRT solutions are shedding both energy and angular momentum by an amount that increases exponentially.

(iii) The instability can be quite strong, depending on the particular combination of parameters that define the geometry. More importantly, the instability is robust, in the sense that it exists for a wide range of parameters.

(iv) With  $m = n + 1$ , the JMaRT solutions are supersymmetric and so must be stable. It is a consistency check of our analysis then that we find no instability in this case. As commented in Section IV, when  $m = n + 1$  the potential  $V_+$ , as given by Eq. (40), is always positive. Hence there are no negative  $\Sigma_\psi$  modes which could intersect the potential well of  $V_+$  and the SUSY geometry is stable as required.

In our analysis, we have focused on the special case  $\lambda = 0$  and  $m_\phi = 0$ , to simplify the relevant equations. In fact, the ergoregion instability persists when either or both of these parameters are nonvanishing. A discussion of the general situation is given in Appendix C. The result is most simply understood from the point of view of the WKB approach. Then all of the additional contributions to the effective potential (29) introduced by a nonvanishing  $m_\phi$  or  $\lambda$  are suppressed by inverse powers of  $m_\psi$  and so can certainly be neglected in the limit of large  $m_\psi$ . One can further check that the instability exists over some range even when  $m_\psi$  does not dominate the other two. One distinguishing feature of  $\lambda \neq 0$  is that asymptotically the scalar modes have an effective mass in five dimensions. In our analysis, this is reflected in the fact that asymptotically  $V_\pm \rightarrow \pm|\lambda/m_\psi|$  and so there is an additional barrier for the modes to tunnel out to infinity. However, for sufficiently large  $m_\psi$ , such tunnelling is possible. One other interesting point about the large  $m_\psi$  regime is that unstable modes appear with either sign of  $m_\phi$  and  $\lambda$ . Hence while for the modes on which we have focussed, the instability is ‘powered’ by  $J_\psi$  and results in decreasing this angular momentum, there are unstable modes which may at the same time increase  $|J_\phi|$  and/or  $P$ .

Adding a mass for the scalar field modifies the potentials  $V_\pm$  in essentially the same way as having nonvanishing  $\lambda$ . Hence we expect the ergoregion instability will even appear for massive fields, at least in modes with sufficiently large angular momentum. As described in section IIB, the arguments given by Friedmann [26] are quite general and so we expect the ergoregion instability to appear for higher spin fields as well. In particular, we expect the fields of the low energy type IIb supergravity will generically experience this instability. Having said that the ergoregion instability is robust, we must also add that it can be suppressed in certain parameter regions. In particular, one finds that the instability timescale becomes extremely long in the regime where  $Q_1$  and  $Q_5$  are much larger than the other scales. Further we add that in the decoupling limit where one isolates an asymptotically  $\text{AdS}_3$  core [1], the ergoregion instability is absent. The simplest way to understand this result is that the  $\text{AdS}_3$  core has a globally timelike Killing vector [1] and so there is a ‘rotating’ frame where we can define all energies to be positive. One can also explicitly verify the absence of an ergoregion instability in the core solutions by directly applying the analysis used in this paper to those backgrounds.

The JMaRT geometries (both supersymmetric and non-supersymmetric) also have damped modes, *i.e.*, modes (12) for which the imaginary part of  $\omega$  is negative. As per the WKB analysis, these are modes with positive  $\Sigma_\psi$  below the local maximum of  $V_+$  that tunnel out to infinity through  $V_+$  — see Fig. 4.

As emphasized previously, we can also find purely bound states (*i.e.*, nonradiative modes) with  $\kappa^2 \propto \omega^2 - \lambda^2 < 0$ . With some fine-tuning, it may also be possible to find geometries which support bound states with  $\kappa = 0$ . These nonradiative modes are described in Appendix D. The typical situation for such modes is sketched in Fig. 5. As already noted above when  $\lambda \neq 0$ , asymptotically  $V_\pm \rightarrow \pm|\lambda/m_\psi|$  and so there is a finite potential barrier at infinity.

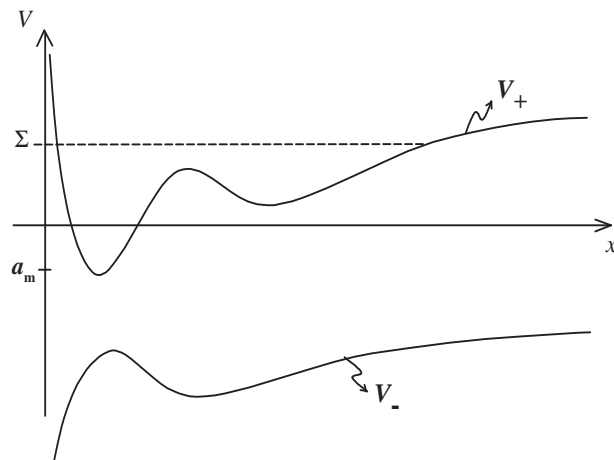


FIG. 5: Qualitative shape of the potentials  $V_+$  and  $V_-$  when  $\omega^2 - \lambda^2 < 0$ . These are the purely bound states that are discussed in Appendix D.

If this barrier is sufficiently large relative to  $\Sigma_\psi = \omega/m_\psi$ , bound states can arise. These bound states can also be negative energy states, as can be seen with the energy integral (7). The absence of such negative energy modes which do not radiate at infinity was central to Friedman’s general argument for the ergoregion instability. In [26], he did not find any such nonradiative modes because he only considered the massless fields for which there is no potential barrier at infinity. Note, however that the current situation is more complicated because the KK-momentum of the background, as well as the angular momenta, contribute to the presence of an ergoregion.

The appearance of negative energy states in the presence of an ergoregion can be anticipated from a geodesic analysis [27]. By definition, the Killing vector  $t^a$ , which generates asymptotic time translations, becomes space-like inside the ergosphere. Hence (time-like or null) geodesics can have either positive or negative energy,  $e = -t \cdot u$ , in this region. However, asymptotically only positive energy (*i.e.*, future-oriented) geodesics are physical. Therefore any negative energy geodesics must be confined to circulate within the ergoregion. Of course, in a black hole background, such geodesics would ‘disappear’ behind the event horizon. However, for horizon-free geometries, such as the JMaRT solutions, they are stable bound orbits and so it is natural to find bound states in the context of a field theory analysis. However, the question then becomes whether the analogous modes of the field ‘fit’ inside the ergoregion or whether they ‘leak’ out to infinity, *i.e.*, whether a negative energy bound state or an ergoregion instability results. A more thorough examination of the bound states shows that the negative energy bound states are characterized by having  $\Sigma_\eta = \omega/\lambda < 0$  while the ergoregion instability is associated with modes where  $\Sigma_\psi = \omega/m_\psi$  and/or  $\Sigma_\phi = \omega/m_\phi$  are negative – see Appendices C and D. Hence as the geodesic analysis would suggest the negative energy modes have a negative pattern speed or phase velocity, but the KK-momentum modes tend to lead to bound states while the spinning modes are related to instabilities.

The presence of negative energy bound states can also be expected to enhance the decay of these horizon-free geometries. The analysis of the ergoregion instability (considered in this paper) is only at the level of linearized test fields. Generically any theory coupling to gravity will also have nonlinear interactions (*e.g.*, even the free scalar considered here has nonlinear couplings with gravitons). These nonlinear couplings might be expected to lead to processes, where positive energy modes are radiated at infinity while negative energy modes are populated within the ergoregion. However, one should note that the negative energy modes are exponentially decaying at large radius — see Appendix D — while the positive energy modes are power-law suppressed inside the ergoregion. Hence the overlap of these modes is expected to be small, which will suppress this nonlinear contribution to the decay.

We now turn to consider the endpoint of the ergoregion instabilities. As emphasized before, the presence of these instabilities relies on two key ingredients, namely, the geometry has an ergoregion but it does not have an event horizon. Hence the resulting decay process could be terminated either by the disappearance of the ergoregion or the appearance of a horizon. However, the unstable modes radiate with a positive energy density asymptotically which is compensated for by a negative energy density inside the ergoregion — as could be seen in Eq. (7). Hence the onset of the ergoregion instability produces a(n exponential) build-up of negative energy near the core of the JMaRT solutions. Therefore it seems unlikely that an event horizon will form since the latter is typically associated with a large build-up of positive energy density. This reasoning then suggests that the decay must terminate with the disappearance of the ergoregion. The supersymmetric D1-D5-P microstate geometries [15, 18–20] are all free of an ergoregion and hence it is natural to suppose that these are at the endpoint of the ergoregion instabilities. Of course,

these solutions offer a huge family of possible endpoints and the precise one that forms will depend on the details of the decay process, beyond the linear regime considered here — although as we are only considering the classical evolution, it is in principle possible given a certain set of initial conditions. Of course, we can expect that the final mass should be close to the BPS mass determined by the charges of the initial JMaRT solution, *i.e.*,  $E = \pi/4G_5 [Q_1 + Q_5 + Q_P]$ . Although even here, we can only say ‘close’ as we know that the unstable modes with  $\lambda \neq 0$  (and *either* sign of  $\lambda$ ) occur which may modify the final value of  $Q_P$ . Similar comments apply for the angular momenta,  $J_\psi$  and  $J_\phi$ . We also observe that there is no reason to expect that the decay process will lead to an endpoint within the family of supersymmetric JMaRT solutions. Of course, at the level of the present discussion, we cannot rule out that the endpoint is only a nearly supersymmetric solution (or that this would be the effective endpoint). Our expectation is that such solutions will have a ‘small’ ergoregion and that the instability might be eliminated (or strongly suppressed) before the ergoregion precisely vanishes.<sup>10</sup>

The stability analysis of the JMaRT solitons [1] is relevant for the stringy tachyon decays discussed recently in [29]. Originally, [30] considered tachyon condensation in certain D1-D5 black string backgrounds where tachyonic string winding modes can occur if one chooses antiperiodic boundary conditions for the fermions around the circle on which the black string is compactified. The latter choice necessarily restricts the scenario to a non-supersymmetric sector of string theory which already suffers from various instabilities [41]. Ref. [29] considered adding angular momentum to the black strings. In this case, it was shown that string modes winding certain compact circles near the horizon can be tachyonic even when the asymptotic fermion boundary conditions are supersymmetric. The relevant point for the present discussion is that the endpoint of the tachyon condensation is in general one of the non-supersymmetric JMaRT solitons. Now, in this paper, we have shown that these solitons are themselves unstable and so they will not be the final endpoint of these decays. Instead, the ergoregion instability will continue the decay process and as suggested above, will likely terminate with a supersymmetric microstate geometry.

We would now like to consider the implications of ergoregion instabilities for Mathur’s fuzzball program of describing black holes in terms of an ensemble of microstate geometries. If this program is to succeed it must supply a description of both supersymmetric and also non-supersymmetric black holes. At first sight, it may appear that constructing non-BPS microstate geometries is not possible. In particular, non-BPS states will decay and so it is not clear that there should be stationary geometries to describe them. However, the JMaRT solutions provide an explicit example indicating that this is not really a problem. In fact, the decay of non-BPS microstates was already considered in the D-brane description of nonextremal black holes [3]. In that context, it was seen as a success of the string theoretic approach as this instability had an interpretation in terms of Hawking radiation [42–44]. Of course, Hawking radiation is a quantum effect in the black hole background and so presents no obstacle to the construction of classical supergravity solutions which are static or stationary.

It is perhaps useful to remind ourselves as to how this distinction arises. The classical limit can be understood as the limit where the string coupling  $g_s$  is vanishingly small [43]. However, the interesting classical solutions are those which correspond to states where the various quantum numbers are extremely large. That is,  $n_1, n_5 \propto 1/g_s$  and  $n_p, J_\psi, J_\phi \propto 1/g_s^2$  while  $g_s \rightarrow 0$ . These scalings are chosen to ensure that the gravitational ‘footprint’, *i.e.*,  $Q_1, Q_5, Q_P, a_1$  and  $a_2$ , associated with each of these quantum numbers remains finite. However, in this limit, the ADM energy of the system diverges with  $E \propto 1/g_s^2$ . As the energy is a dimensionful quantity, this can be accommodated by changing the units with which energies are measured in the classical limit. Essentially this divergence is associated with the divergence of the Planck mass, which does not serve as a useful reference scale in classical gravity. Now the decay rate of the nonextremal D1-D5-P black holes can be computed in a straightforward manner [43, 44]. The key point, however, is that the final expression for  $dE/dt$  is expressed in terms of geometric quantities and is independent of  $g_s$ . Therefore in the classical limit, the rate of energy loss remains finite in stringy units but becomes vanishingly small when measured against the fiducial energy scale that was established for classical physics. Hence the non-BPS black holes become stable in the classical regime.

We note that the ‘straightforward’ calculations of the decay rate referred to above can be performed either in the framework of a microscopic D-brane perspective or of the gravitational perspective of Hawking radiation. The surprising result is that the results of both analyses agree precisely [43, 44], including greybody factors, at least in the so-called ‘dilute gas’ approximation [45]. However, even though suggestive arguments can be made in this regime [46], this remarkable agreement remains poorly understood. As the JMaRT solutions are horizon-free, the gravitational calculation of the decay rate would have to be modified. Using the connection between absorption and emission rates, it is possible that absorption calculations along the lines of those presented in [1] could be extended to yield

---

<sup>10</sup> We should note that the JMaRT solutions begin in a low-mass regime where  $M^2 < (a_1 - a_2)^2$ , however, if the ergoregion instability sheds the background angular momentum efficiently then the system will evolve to a regime where black holes can form. Hence we can not rule out the appearance of an event horizon – we thank Simon Ross for correspondence on this point.

the desired decay rate. On the other hand, the underlying microscopic states for the JMaRT solutions were already identified in [1]. Hence one can use microscopic techniques to estimate the decay rate expected for these solutions. The result is  $dE/dt \sim Q_1 Q_5 (m - n)^6 / R^6$  and again this quantity remains finite as  $g_s \rightarrow 0$ . Therefore we can again ignore this decay channel for the classical JMaRT solutions.

However, the ergoregion instability investigated in this paper is a classical instability and so should not be associated with the decay discussed above. We should also note that the form of these two instabilities differs. Above one is considering the spontaneous decay of the system while the classical instability really corresponds to a decay that results when the initial data does not precisely match that of the JMaRT solutions. Of course, in the quantum regime, the same modes associated with the ergoregion instability will give rise to spontaneous decay due to quantum fluctuations of the background.<sup>11</sup> However, the latter will again be suppressed in the  $g_s \rightarrow 0$  limit. This reflects the fact that the background can be prepared with arbitrarily accurate precision in the classical limit and so it should be possible to produce an arbitrary suppression of ergoregion instability. Alternatively, working in the classical limit, we can regard the ergoregion instability as a property of how the JMaRT solutions interact with external sources. That is, generically if an external wave packet impinges on one of the non-supersymmetric JMaRT configurations, it will produce a dramatic decay of the original background. Hence this instability seems to present a major challenge for the fuzzball description of black holes.

We have argued that the ergoregion instability is a robust feature of the non-supersymmetric JMaRT solutions over a wide range of parameters. Given general arguments along the lines of [26], we also expect that this instability will be a generic feature of any smooth horizon-free geometries which describe microstates which are non-BPS and carry significant angular momentum (and hence have a macroscopic ergoregion). Therefore if a nonextremal D1-D5-P black hole is to be described by a coarse-grained ensemble fuzzball, it seems that that the classical black holes must suffer from an analogous instability. While the presence of an event horizon eliminates the possibility of an explicit ergoregion instability, there are, in fact, a number of potential instabilities which might afflict these black holes and possibly reproduce the same physics:

**a) Superradiant Instability:** Spinning nonextremal black holes will exhibit superradiant scattering, where an incident wave packet can be reflected with a stronger amplitude. Superradiance by itself does not provide a classical instability, but an instability can arise if the scattered modes are reflected back to rescatter, as described in Section II. This scattering was considered for higher dimensional spinning black branes [33] and there it was found that when the noncompact space has more than four dimensions, this instability does not arise. Explicitly analyzing the present D1-D5-P black string again seems to indicate the absence of an instability [47].

**b) Gyration Instability:** Considering supersymmetric D1-D5-P black strings, it was found that above a certain critical angular momentum a straight black string is unstable towards carrying the angular momentum in gyrations of the horizon [48]. This instability should also appear in non-supersymmetric configurations and so would present an instability at large values of the angular momentum.

**c) Gregory-Laflamme Instability:** The relevant configurations are black strings and so are expected to suffer from the Gregory-Laflamme instability [49] in two ways. The first is the usual instability of long wavelength modes along the string. Of course, this instability can be eliminated by reducing the radius of the compactification along the string. For a fixed radius, it is also suppressed by the boosting along this direction which induces the KK-momentum [50]. This instability is not related to the angular momentum carried by the black string or the presence of an ergoregion, but we list it here for completeness.

**d) Ultra-spin Instability:** In six or higher spacetime dimensions, one can find black hole solutions with an arbitrarily large spin per unit mass [36]. However, it was argued [51] that a Gregory-Laflamme-like instability will arise to dynamically enforce a Kerr-like bound in these cases. While this analysis does not directly apply in five dimensions, entropy arguments suggest an analogous instability still exists and will lead to the formation of a black ring if the angular momentum is too large [52].

While there are several possibilities for instabilities of a black string in six dimensions, it seems that none of these can reproduce the physics of the ergoregion instability which will afflict the non-BPS microstate geometries. This observation relies on the fact that these instabilities have a different character at a very basic level. The ergoregion instability might be termed a radiative instability, in that, the instability is by definition connected to modes that radiate at infinity. In contrast, the four instabilities considered above for black strings can be termed internal instabilities. That is, these instabilities are primarily associated with a rearrangement of the internal or near-horizon structure of the black string. While these instabilities will be accompanied with some radiation at infinity, this will be a secondary effect with these instabilities. Therefore it seems that emulating the ergoregion instability in a nonextremal black string background will require the discovery of a new kind of instability. While we are performing

---

<sup>11</sup> In [1] it was erroneously assumed that all of these geometries have an AdS<sub>3</sub> core to argue that such emissions would not occur.

a detailed analysis of the nonextremal D1-D5-P black string, our preliminary results indicate that no such instability arises [47].

We also note in passing that at the same time the microstate geometries should be able to emulate any instabilities found in the black string backgrounds. In particular, the Gregory-Laflamme instability is a robust instability that will afflict these backgrounds for sufficiently large  $R$ . In the microstate geometries, one should then find unstable modes carrying KK-momentum which are confined near the core of the soliton. We have studied bound states for a test field in the JMaRT solutions, as described in Appendix D. While the modes we identified only arise for nonvanishing KK-momentum as desired, they are all stable, *i.e.*, they have real frequencies. Hence they can not serve as the analog of the Gregory-Laflamme instability in the non-supersymmetric JMaRT solutions. However, the latter would be a gravitational instability, *i.e.*, it should not be expected to appear as a scalar test field, and so this question requires further investigation.

A possible reconciliation of these ideas with the fuzzball proposal would be that the microstate geometries could provide an accurate description of a black hole but only over a long but finite time. In the context of the  $\text{AdS}_3/\text{CFT}_2$  duality, some evidence for such a picture has recently been found [53]. With this new point of view, a key question is to determine the timescale over which microstate geometries cannot be distinguished from black holes. One suggestion [53] is that it should be of the order of the recurrence time, which would be exponential in the relevant quantum numbers. An alternative suggestion might be that the timescale is associated with Hawking evaporation which would involve (inverse) powers of the quantum numbers. However, note that both of these suggestions diverge in the classical limit. Hence the ergoregion instability found here seems to be in conflict with both of these suggestions. While the instability timescale is certainly very long in certain parameter regimes, it is a classical timescale, *i.e.*, it is finite in the classical limit. Hence our results would suggest that spinning microstate geometries and black holes should be distinguishable on a large but classically finite timescale.

However, one must ask how characteristic our results for the JMaRT solutions will be of generic microstate geometries. In particular, we note that the CFT states corresponding to the JMaRT solutions are exclusively in the untwisted sector [1, 19, 54]. On the other hand, the majority of microstates accounting for the entropy of the black strings are expected to be in a (maximally) twisted sector [11]. From a geometric point of view, we would observe that the JMaRT solutions have all the same Killing symmetries as the D1-D5-P black holes, while the generic microstate geometry is expected to have a complex nonsymmetric core. Therefore it is not unreasonable to expect that the ergoregion instability timescales found for the JMaRT solutions will not be characteristic of the microstate geometries that make up ‘most’ of the black hole.

One possibility might be the generic non-BPS geometries do not have ergoregions despite the fact that they carry angular momentum. However, we argue that such a scenario is implausible as follows: The fuzzball description would now require that both the horizon and the ergosphere arise as effective surfaces in ‘coarse-graining’. However, quantum fluctuations must then extend out to the ergosphere. In particular, these fluctuations extend to regions of the spacetime which should be causally accessible to asymptotic observers on finite classical timescales. Hence it seems inconsistent to say that the underlying microstate geometries are hidden from asymptotic observers in this scenario.

Hence as argued above, if the non-BPS microstate geometries are horizon-free with an ergoregion, they should expect an ergoregion instability. However, it may be that instability timescales calculated for the JMaRT solutions are not representative of those for typical microstate spacetimes. In particular, the latter should have complicated throats — as seen in their supersymmetric counterparts [13–15] — which would emulate the absorptive behavior of a black hole horizon. Hence it might be expected that the relevant timescales are extremely long. An important question is then whether the instability timescale is classically finite or not. That is, will this timescale diverge as the quantum numbers grow as described above. Certainly finding more generic non-BPS microstate geometries is an essential step towards resolving this issue.

In closing, we note that in the context of the AdS/CFT, a complete description has been produced for half-BPS microstate geometries with  $\text{AdS}_5$  [55] and  $\text{AdS}_3$  [56] asymptotics. This framework has given rise to an interesting program of semi-classical quantization [53, 57, 58] and a coarse-graining description of spacetime geometry [59]. With this program in mind, it is useful to recall the role of the smooth horizon-free microstate geometries in Mathur’s ‘fuzzball’ program [11].

The BPS microstate geometries for the D1-D5 system can be derived by studying the F1-P geometries and applying a series of duality transformations [15]. There the winding and wave numbers might be quantized by the geometry but classically the amplitudes of the string excitations are continuous variables. Solutions where select modes are excited with a large amplitude can then be seen as ‘coherent states’ of the underlying quantum theory. Such solutions may be further useful to understand certain properties of typical microstates, *e.g.*, their transverse size [11]. However, ultimately a generic state will have a vast number of modes excited with very few quanta and hence the corresponding ‘spacetime’ will not be accurately described by a classical geometry. However, the family of classical geometries still serve as a guide to the classical phase space which must be quantized [58].

In the present context, we wish to go beyond the BPS sector where program is much less developed. In particular, we still face the challenge of constructing a more or less complete family microstate geometries. The existence of the JMaRT solutions indicate that at least certain non-BPS states can be described by classical geometries. However, it is not at all clear how large a class of nonsupersymmetric smooth horizon-free geometries exists. Going beyond the present special class of solutions will probably call for the development of new solution-generating techniques, but the JMaRT geometries offer hope that a broader class of nonsupersymmetric solutions can be found. This will certainly be an intriguing direction for further research and will undoubtedly lead to interesting new insights and discoveries.

### Acknowledgements

It is a pleasure to acknowledge Vijay Balasubramanian, Thomas Levi, Donald Marolf, Samir Mathur and Simon Ross for interesting comments and discussions. Research at the Perimeter Institute is supported in part by funds from NSERC of Canada and MEDT of Ontario. RCM is further supported by an NSERC Discovery grant. VC and OJCD acknowledge financial support from Fundação para a Ciência e Tecnologia (FCT) - Portugal through grant SFRH/BPD/2004. OJCD also acknowledges CENTRA - Centro Multidisciplinar de Astrofísica, Portugal for hospitality. J LH was supported by an NSERC Canada Graduate Scholarship.

### APPENDIX A: WKB MATCHING

In this appendix we use the usual WKB wavefunctions and WKB connection formulae at the turning points to relate the amplitude of the wavefunctions in the four distinct regions of the scattering problem and, in particular, to derive (47). The four WKB regions are (see Fig. 1): Region I, the innermost forbidden region ( $0 < x < x_0$ ); Region II, the allowed region where  $V_+$  is below  $\Sigma_\psi$  ( $x_0 < x < x_1$ ); Region III, the potential barrier region where  $V_+$  is above  $\Sigma_\psi$  ( $x_1 < x < x_2$ ); and Region IV, the external allowed region where  $\Sigma_\psi$  is below  $V_-$  ( $x_2 < x < \infty$ ). The WKB wavefunctions in region I and in region IV were already written in (45) and (46), respectively, and in regions II and III they are given by

$$H_{\text{II}} \simeq \frac{C_2}{m_\psi^{1/2} T^{1/4}} \exp \left[ i m_\psi \int_{x_1}^x \sqrt{T} dx \right] + \frac{C_3}{m_\psi^{1/2} T^{1/4}} \exp \left[ -i m_\psi \int_{x_1}^x \sqrt{T} dx \right], \quad (\text{A1})$$

$$H_{\text{III}} \simeq \frac{C_4}{m_\psi^{1/2} |T|^{1/4}} \exp \left[ -m_\psi \int_{x_1}^x \sqrt{|T|} dx \right] + \frac{C_5}{m_\psi^{1/2} |T|^{1/4}} \exp \left[ m_\psi \int_{x_1}^x \sqrt{|T|} dx \right]. \quad (\text{A2})$$

Using the WKB connection formulae in each turning point,  $x_0$ ,  $x_1$  and  $x_2$ , we can find the relations between the amplitudes  $C_i$ 's ( $i = 1, \dots, 7$ ) of the several regions, yielding:

$$C_2 = C_1 e^{i\gamma}, \quad C_3 = C_1 e^{-i\gamma}. \quad (\text{A3})$$

$$C_4 = \frac{1}{2} \left( C_2 e^{-i\pi/4} + C_3 e^{i\pi/4} \right), \quad C_5 = i \left( C_2 e^{-i\pi/4} - C_3 e^{i\pi/4} \right), \quad (\text{A4})$$

$$C_6 = \left( \frac{iC_4}{2\eta} + C_5 \eta \right) e^{-i\pi/4}, \quad C_7 = \left( -\frac{iC_4}{2\eta} + C_5 \eta \right) e^{i\pi/4}, \quad (\text{A5})$$

with  $\gamma$  and  $\eta$  defined in (48) and (49), respectively. Finally, combining these three sets of relations yields (47).

### APPENDIX B: DETAILS OF NUMERICAL ANALYSIS

In this Appendix we discuss some issues related to the precision used in the numerical computations. Even though the very small imaginary parts of  $\omega$  are well described by both approximations, for completeness we show that they are not a numerical artifact due to loss of precision in our numeric routines or a by-product of using the approximate solutions to specify the boundary conditions. In Fig. 6 we plot the imaginary part of  $\omega$  for several values of the number of digits of precision used in the calculation. We use the same parameters as before and set  $N = 0$ ,  $l = m_\psi = 4$ . We



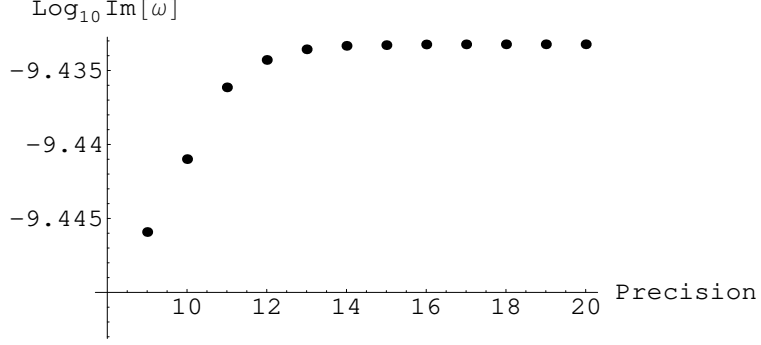


FIG. 6: Effect of increasing digits of precision used on imaginary part of eigenvalue.

see, as one would expect if the imaginary part were actually non-zero, that the eigenvalue converges to a constant value when the number of digits is larger than the size of the imaginary part.

With only the asymptotic form of the solutions to specify the boundary conditions we are not actually setting the coefficient on the divergent term to zero. Instead, there will always be some amount of the divergent solution in the numerically defined solution. The suppression of the divergent term is dependent on how deep into the asymptotic region we choose to apply the boundary condition. To ensure that these small divergent terms are not causing any errors we study the effect of varying the point at which we apply the boundary conditions. This has been shown in Fig. 7 on the left and right. In both cases, we again see that the eigenvalue converges to a constant value as we increase the accuracy of the calculation.

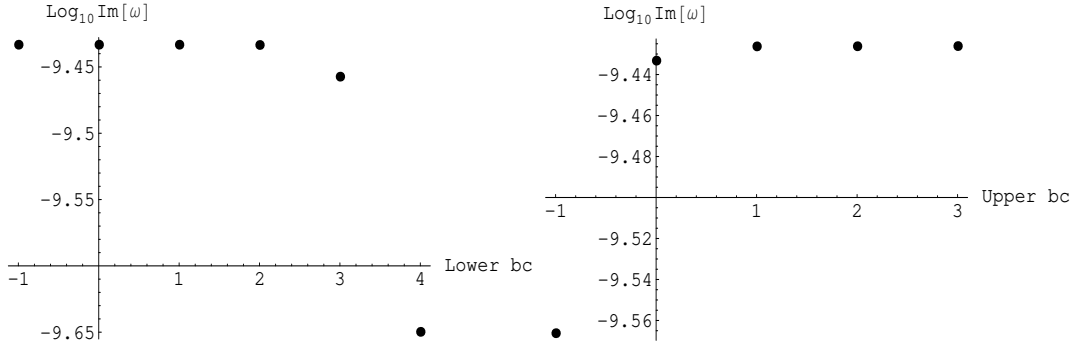


FIG. 7: On the left we vary the point at which the inner boundary condition is applied,  $\log_{10} x_0$ , from the value at which  $(x\kappa^2)/(\zeta^2/x) = 10^{-5}$ . On the right, we do the same for the outer condition from the value at which  $(x\kappa^2)/(\zeta^2/x) = 10^3$ .

### APPENDIX C: DETAILED ANALYSIS OF THE INSTABILITY

The existence of a solution to the matching procedure can be reduced to the requirement that a number of constraints be satisfied. The difficulty one runs into when trying to discuss the general properties of these solutions is that while all the parameters appearing in the various equations are uniquely determined by the set  $\{Q_1, Q_5, R, m, n\}$ , it is difficult to write explicit expressions for them. In this sense, the fact that the parameters (9) can be written in such a simple form is really quite surprising since all are proportional to  $M$ , which can at best be defined implicitly in terms of the above parameters.

Hence it is useful to have an approximation for  $M$  that allows one to understand the general behavior of the various

parameters. Surprisingly there is quite a simple approximate solution given by

$$M \approx 2(s^{-1} - s) \frac{Q_p}{1 + nm \left( \frac{Q_1 + Q_5}{R^2} \right)}, \quad (\text{C1})$$

where we recall that  $Q_p = nmQ_1Q_5/R^2$ . For most parameter values, this expression is accurate on the order of a few percent. When one of the D-brane charges, say  $Q_1$ , grows much larger than  $Q_5 \sim R^2$  this approximation can break down, though only by a few percent times  $(m - (n + 1))$ . Similar problems appear when  $R^2 \gg Q_1 \sim Q_5$ , in this case the error appears to be of the same order. The important thing to note is that it gives the correct scaling of  $M$  with the various parameters in all situations. In most cases, except those noted previously when  $m \gg n$ , it also gives the correct order of magnitude. Treating  $m$  as a continuous parameter, the approximation appears to produce the approach to the supersymmetric limit exactly.

Using this, one can approximate, or at least bound, the parameters appearing in the solutions.

$$\varrho = \frac{c_1^2 c_5^2 c_p^2 - s_1^2 s_5^2 s_p^2}{s_1 c_1 s_5 c_5} \approx \frac{s^{-1} + s}{2} \left( 1 + nm \frac{Q_1 + Q_5}{R^2} \right) \quad (\text{C2})$$

$$\begin{aligned} \varepsilon &\leq \frac{1}{R^2} \left( Q_1 + Q_5 + Q_p + M \left( 1 - \frac{nms^2}{(s^{-2} - s^2)^2} \right) \right) \\ &\approx \frac{1}{R^2} \left( Q_1 + Q_5 + Q_p + \frac{2Q_p}{1 + nm \frac{Q_1 + Q_5}{R^2}} \left[ \frac{nm(1 - s^4)^2 - s^6}{nms(1 - s^4)(1 + s^2)} \right] \right) \end{aligned} \quad (\text{C3})$$

$$\begin{aligned} \vartheta &\leq \frac{Q_p}{Q_1 Q_5} (Q_1 + Q_5 + M) \\ &\approx \frac{Q_p}{Q_5} + \frac{Q_p}{Q_1} + 2 \frac{Q_p^2}{Q_1 Q_5} \frac{s^{-1} - s}{1 + nm \frac{Q_1 + Q_5}{R^2}} \end{aligned} \quad (\text{C4})$$

In the above, the inequalities result from writing  $s_i^2 \leq s_i c_i = Q_i/M$ , in particular they become exact for the extremal limit. From the expression for  $\varepsilon$  one sees that it is finite, and in fact positive for all  $m \geq n + 2$ . It is only in the extremal limit that  $\varepsilon \rightarrow -\infty$ , which precludes any possible instability. One may also check from these forms that  $\varepsilon/\varrho^2 \ll 1$  for all values of the parameters, which can be verified numerically for sets of parameters in which the approximations are less trustworthy. In what follows then we will neglect  $\varepsilon$  where consistent.

The timescale of the instability is an increasing function of  $\nu$  which, given the above considerations, is given by

$$\nu \approx -\lambda \frac{Q_p}{\varrho R^2} + \sqrt{\lambda \frac{Q_p}{\varrho R^2} \left( \lambda \frac{Q_p}{\varrho R^2} + 2c \right) + \nu_0^2 - \frac{\varepsilon}{\varrho^2} c^2}. \quad (\text{C5})$$

Unfortunately, we cannot make any definite statements about the size of  $Q_p/\varrho R^2$  like we did previously for  $\varepsilon$  since it can be made arbitrarily large or small just by varying  $R$ . At this point we could use the explicit forms for  $\nu_0^2$  and  $c$  to discuss the general properties of the solutions. Instead we will for now set  $\lambda = 0$  to make the discussion more transparent. Non-zero  $\lambda$  will not change the general features of the solutions.

Setting  $\lambda = 0$ , the above expression for  $\nu$  simplifies quite a bit

$$\nu \approx \sqrt{\nu_0^2 - \frac{\varepsilon}{\varrho^2} c^2}. \quad (\text{C6})$$

We are now in a position to discuss the behavior of the timescale for various different solutions. Recall that the timescale for the instability is smallest when  $\nu$  is smallest. Therefore the instability will be strongest when  $\nu_0 = l + 1$  is smallest. This, of course, does not mean that we should necessarily consider solutions with  $l = 0$ , in fact we shall see in a moment that such solutions are not possible. More precisely the minimum value of  $l$  for which all the constraints can be satisfied will lead to the most unstable solution.

Similarly, when  $c^2$  or  $\varepsilon/\varrho^2$  is largest the instability be the strongest. We shall deal with  $c$  next, but for now it is sufficient to note that it is only dependent on  $m$  and  $n$ . Observe from (C4) that for fixed  $R$ ,  $\varepsilon/\varrho^2$  varies roughly like the inverse of the charges, therefore when one considers limits in which the charges grow, the timescale of the instability diverges. Similar arguments hold when  $R$  is vastly different from the charges, we find that  $\varepsilon/\varrho^2$  shrinks and the lowering effect of  $c^2$  is diminished. It appears then that the instability will be strongest when  $Q_1 \sim Q_5 \sim R^2$ .

To discuss the relative effect of  $c$  we should return to the constraints. These also simplify when we set  $\lambda = 0$  and we may consider the simpler constraint  $c - \nu_0 > 0$ . The exact form that  $c$  takes is dependent on the sign of  $\zeta$ . By

studying the constraints, it turns out that solutions with  $\zeta > 0$  will in general exist, but for larger values of  $l$  than when  $\zeta < 0$ . Given the considerations above, the effect of these modes will be subdominant. We therefore focus on  $\zeta = -nm_\psi + mm_\phi < 0$  which implies that  $m_\psi > m_\phi$ . One can then write the constraint as

$$c - \nu_0 = [(m - n)(m_\psi + m_\phi) - (2N + 1)] - [l + 1] \quad (\text{C7})$$

$$= (m - (n + 1))(m_\psi + m_\phi) - (l - m_\psi - m_\phi) - 2(N + 1) > 0. \quad (\text{C8})$$

Further, it can be shown that when this is satisfied, the other constraints follow automatically. The last two bracketed terms in the final line are positive, so a solution requires that  $m_\psi + m_\phi > 0$ , implying that  $m_\psi$  must be positive. This is a general result that is also obtained when  $\zeta > 0$  or  $\lambda \neq 0$ . When  $c$  is largest, the timescale will be shortest, therefore the lowest harmonic  $N = 0$  will lead to the strongest instability. One can also make  $c$  large by choosing  $m_\psi$  and  $m_\phi$  as large as large as possible,  $m_\psi + m_\phi = l$ , but taking  $l$  large will not necessarily give us a very unstable mode because as noted before it will cause  $\nu_0$  to rise which has an opposing effect. Since  $c^2$  enters weighted by  $\varepsilon/\varrho^2$ , the more important contribution will be that from  $\nu_0$  and the net effect is a less unstable mode. Finally, note that  $m_\phi$  and  $m_\psi$  appear symmetrically in  $c$ , so that the value of  $\nu$  will be independent of the partition of  $l$  into  $m_\phi$  and  $m_\psi$ . This does not mean that the timescale will be independent of this partition since it is a weakly shrinking function of  $|\zeta|$  for fixed  $\nu$ . When  $|\zeta|$  is maximized the timescale will be the shortest, which is the case when  $m_\psi = l, m_\phi = 0$ .

To summarize then, for a fixed mode that solves the constraints, the instability will be strongest when  $Q_1 \sim Q_5 \sim R^2$ . On the other hand, when we fix a particular background, the instability with  $\lambda = 0$  will be strongest when  $l = m_\psi$  is as small as possible and  $m_\phi = 0$ .

Finally then we may discuss the solutions for which  $\lambda \neq 0$ . It turns out that the various scalings of the other parameters appears not to be changed. When  $\lambda \neq 0$ , the constraint  $c^2 - \nu_0^2 > 0$  becomes easier to satisfy since  $c$  picks up a contribution proportional to  $\vartheta\lambda$  while the contribution to  $\nu_0$  is smaller. The tougher constraint to satisfy is then the one that implies  $\omega^2 > \lambda^2$ . When all other parameters are fixed, this places upper and lower bounds on (*i.e.*, we allow negative  $\lambda$ )  $\lambda$ . We will not go into detail here, but instead note one can always find solutions with non-zero  $\lambda$  by going to sufficiently large angular momentum,  $l$ .

When studying the characteristic time for the instabilities, one finds that the timescale decreases as  $\lambda$  is raised, but reaches a maximum shortly before reaching the upper bound. For negative values, on the other hand, the timescale is a constant decreasing function of  $\lambda$ . As mentioned, solutions with non-zero  $\lambda$  require larger values of  $l$  than when  $\lambda = 0$ . Though larger  $l$  tends to increase the timescale, the overall effect of going to larger  $l$  to accommodate non-zero  $\lambda$  can still lead to shorter timescales.

## APPENDIX D: BOUND STATES

The general radial dependence of the scalar field at large distances from the core is determined by the sign of  $\kappa^2$ . When it is positive, the general solution oscillates with a power-law falloff. This is the behavior that led to the in and outgoing waves at infinity which we have already discussed. The other two possibilities, where  $\kappa^2$  is zero or negative, can lead to quite different behavior. For the former there is an exact solution, while the latter may again be solved with a matched expansion.

### 1. $\kappa^2 = 0$ : Marginally Bound States

By considering the special mode with  $\omega^2 = \lambda^2$ , both the angular and radial equations simplify sufficiently that an exact solution may be found. Such a choice removes all  $\omega$  dependence from the angular equation allowing it to be solved independently. The result is the eigenvalue equation for the harmonics on an  $S^3$ . The exact eigenvalue is  $\Lambda = l(l + 2)$ .

For the radial equation, this choice of mode removes the  $\kappa^2 x$  term; the same condition that previously led to the simplification in the near region. The previous solution in the near region (74) therefore becomes the exact solution in the entire spacetime. This means that asymptotically the equation has a basis of solutions in terms of  $r^{-1 \pm \nu}$ . Ignoring for now the part dependent on the KK momentum, these become  $r^l$  and  $r^{-2-l}$ . These are simply the terms one expects from a Laplace series in four flat spatial dimensions where the angular momentum creates an effective radial potential.

Asymptotic regularity requires that the  $r^{-1+\nu}$  component vanish whenever  $\nu > 1$ , leaving a field that falls off as  $r^{-1-\nu}$ . The natural generalization of Friedmann's analysis of ergoregion instabilities to five-dimensions would involve studying fields that fall off as  $r^{-2}$ , therefore these modes will evade that analysis as long as  $\nu > 1$ . The requirement

that removes the divergent term is similar to that for outgoing modes, except now it is an exact result

$$\nu + |\zeta| \mp \xi = -(2N + 1) , \quad (\text{D1})$$

where  $N$  is a non-negative integer. Here, however, we allow for either of the  $\Gamma$  functions in the denominator to diverge in eq. (76), leading to both possibilities for the sign before  $\xi$ . This is in contrast to the search for unstable modes in which we could neglect one of the possibilities since it was found to correspond to ingoing damped modes. Indeed, since (D1) contains terms linear in both  $\lambda$  and  $\omega$ , one must consider both signs above in order to be consistent with the symmetry under flipping signs as in equation (22).

In total then we have three constraints that must be satisfied for these modes. The first,  $\omega^2 = \lambda^2$ , fixes  $\omega$  to be an integer, meaning that there are no remaining continuous parameters characterizing the scalar field. For a general background then it is unlikely that the remaining constraints, in particular the one defining  $N$ , can be solved by a judicious choice of the integer eigenvalues. On the other hand, fixing the set  $m_\psi, m_\phi$  and  $\lambda$ , there may be families of backgrounds for which these marginally bound states exist.

## 2. $\kappa^2 < 0$ : Bound States

The final possibility for solutions of the radial equation is  $\omega^2 < \lambda^2$ , or  $\kappa^2 < 0$ . As in the case where  $\kappa^2$  is positive, we are unable to find an exact solution, though progress can be made through approximation. In particular, since the effect of the sign of  $\kappa$  is only relevant at large distances from the core, we need only make slight modifications to the matched asymptotic expansion analysis presented earlier.

To begin, we factor out the sign of  $\kappa^2$  by redefining  $\kappa \rightarrow i\kappa$ , giving solutions that are real valued exponentials asymptotically. Requiring regularity therefore leaves only the exponentially damped ‘‘bound states’’, localized near the core region. Explicitly, after having made the redefinition in (77), a convenient basis of solutions is in terms of modified Bessel functions of the first and second kind.

$$h = \frac{1}{\sqrt{x}} [A_1 I_\nu(\kappa \sqrt{x}) + A_2 K_\nu(\kappa \sqrt{x})] . \quad (\text{D2})$$

The first of these diverges at large  $x$  and so we require  $A_1 = 0$  for regularity. For now though, we leave  $A_1$  arbitrary, setting it to vanish only after we have performed the matching.

In the matching region expanding  $I_\nu$  and  $K_\nu$  in the  $x^{\pm\nu/2}$  basis gives

$$h \approx \frac{1}{\sqrt{x}} \left[ \left( \frac{A_1}{\Gamma(1+\nu)} + \frac{A_2 \Gamma(-\nu)}{2} \right) \left( \frac{\sqrt{x} \kappa}{2} \right)^\nu + \frac{A_2 \Gamma(\nu)}{2} \left( \frac{\sqrt{x} \kappa}{2} \right)^{-\nu} \right] . \quad (\text{D3})$$

Note that  $K_\nu$  contains both of these powers of  $x$  when expanded in the overlap region. While the contribution of the positive power to  $K_\nu$  is relatively small, we will keep this contribution until after we perform the matching so that we may see how the approximate solution comes about.

By construction, the solution in the near region (74) is unaffected by the redefinition of  $\kappa$ . Immediately then we may proceed to matching the coefficients on powers of  $x$  in the overlap region. Setting  $A = 1$  in the near region solution, we determine the coefficients  $A_1, A_2$  in the outer region

$$\frac{A_1 (\kappa/2)^\nu}{\Gamma(1+\nu)} = \frac{\Gamma(\nu) \Gamma(1+|\zeta|)}{\Gamma(\frac{1}{2}(1+\nu+|\zeta|+\xi)) \Gamma(\frac{1}{2}(1+\nu+|\zeta|-\xi))} - \frac{\Gamma^2(-\nu) \Gamma(1+|\zeta|) (\kappa/2)^{2\nu}}{\Gamma(\nu) \Gamma(b) \Gamma(\frac{1}{2}(1-\nu+|\zeta|-\xi))} , \quad (\text{D4})$$

$$\frac{A_2 \Gamma(\nu)}{2(\kappa/2)^\nu} = \frac{\Gamma(-\nu) \Gamma(1+|\zeta|)}{\Gamma(b) \Gamma(\frac{1}{2}(1-\nu+|\zeta|-\xi))} , \quad (\text{D5})$$

As before, finding the spectrum of solutions now requires that we find values of the free parameters for which these equations are consistent with the boundary conditions. In particular, we now set  $A_1 = 0$  and therefore ask that the right hand side of (D4) vanishes. Again, rather than find such parameters numerically there is an accurate approximation that comes from noting that consistency requires  $A_2$  be non-zero. This implies that the second term in (D4) must be non-zero and therefore any solution must come from cancellation between the two terms. Since the second term is suppressed by the factor  $\kappa^{2\nu}$ , a comparable suppression must occur in the first term, again requiring the divergence of a  $\Gamma$  function in the denominator. This gives a quantization condition similar to that found previously

$$\nu + |\zeta| \mp \xi \approx -(2N + 1) . \quad (\text{D6})$$

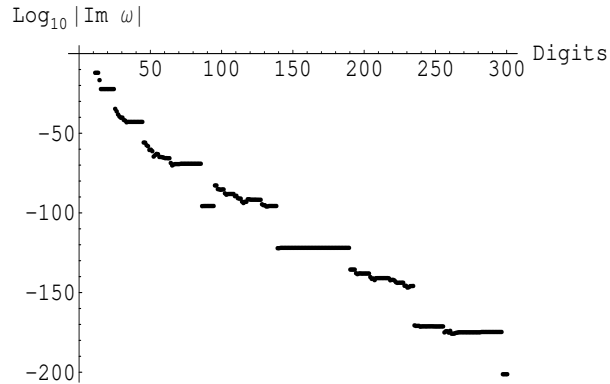


FIG. 8: Variation of the size of the imaginary part of  $\omega$  resulting from the numerical solution of (D4) as the precision is increased.

Here again, the terms linear in  $\omega$  and  $\lambda$  implicit in the above equation – see definitions in eq. (17) — imply that both possibilities are required for consistency with the symmetry (22), though in practice both may not lead to solutions for which  $\omega^2 < \lambda^2$ .

When  $\nu$  is real, this appears to give solutions for  $\omega$  which are purely real. Note, however, we must be careful in solving the constraint since, given the right combination of background charges,  $\nu^2$  could become negative. For an arbitrary frequency in this range, Eq. (D4) will be complex so solutions where  $\omega$  has both real and imaginary parts may be possible. Such solutions cannot be found with the sort of perturbative expansion used in studying the outgoing modes since now it is the real part of  $\nu$  which gains a small correction, while the imaginary part is large. We can therefore no longer consider the behavior near the pole on the negative real axis defined by the real part of Eq. (D6). Instead, we have resorted to searching for these solutions by solving (D4) numerically.

Generically, the root finding algorithm will produce a complex value of  $\omega$  that sets the equation to zero within a specified precision. Since the imaginary part is many orders of magnitude smaller than the real part one should ensure that it really is non-zero and not a numerical artifact. In Figure 8 we show the variation in the size of the imaginary part as a function of the tolerance used in finding the root of (D4). From this plot we see that the imaginary contribution is indeed just an artifact of trying to solve the complex equation. Surprisingly then it appears we can satisfy (D4) with a real value of  $\omega$ , even if that value causes  $\nu^2 < 0$ . That value corresponds to the solution of the equation resulting from taking the real part of the quantization conditions (D6).

Since the condition (D6) is the same as for the outgoing modes, much of the analysis in Appendix C about the existence of solutions applies. The situation is somewhat more complicated in that one now allows modes with positive  $\omega$  and there are two possible solutions corresponding to the two signs in (D6), but the general characteristics of the solutions are the same. In particular, for the outgoing modes it was found that there are upper and lower bounds on the allowable values of  $\lambda$  beyond which  $\omega^2 - \lambda^2$  changes sign. In light of these bound states, we see that the full space of solutions may be considered as split into distinct regions based on the value of  $\lambda$ . There is a small- $|\lambda|$  regime, in which one finds the outgoing unstable modes. This is surrounded, at larger values of  $|\lambda|$ , by a regime where the bound states arise.

This separation of the two types of modes according to the parameter  $\lambda$  makes clear the difference in their origin. In particular, one can always find outgoing unstable modes that do not carry KK momentum, they need only be supplied with sufficient angular momentum. This is in accord with our interpretation of these solutions as the unstable modes predicted by Friedman which result from the existence of the ergoregion. In contrast, bound states will always result as long as  $|\lambda|$  is large enough. This includes modes which carry no angular momentum, thus indicating the important characteristic of these solutions is their KK momentum and the effective five-dimensional mass it induces.

Having established the existence of these bound states we should question just how close to the core region they are bound. The solutions are damped exponentially and so have characteristic size

$$x_{bs}^{-1} \sim \kappa^2 = (\lambda^2 - \omega^2) \frac{r_+^2 - r_-^2}{R^2}, \quad (D7)$$

$$\approx 2(\lambda^2 - \omega^2) \frac{Q_1 Q_5}{(s^{-1} + s) R^2 (R^2 + nm(Q_1 + Q_5))}. \quad (D8)$$

To arrive at the final line we have used the approximation for  $M$  (C1) found in Appendix C. The boundary of the ergoregion, on the other hand, is given by the vanishing of the norm of the Killing vector  $\partial_t$  (10). We ignore the  $a_1, a_2$  dependent contributions appearing in  $f$  to give an outer bound on the size of the ergoregion, given approximately by  $r_{er}^2 \sim Mc_p^2$ . In terms of the variable  $x$  this means

$$x_{er}^{-1} \gtrsim \frac{s^{-2} - s^2}{nm(s^{-2} - s^2)^2 c_p^2 - s^2} . \quad (D9)$$

Whenever  $Q_1$  and  $Q_5$  are much smaller than  $R^2$ , the size of the bound state scales as  $x_{bs}^{-1} \sim Q_1 Q_5 / R^4 \ll 1$ . On the other hand, for large  $Q_1$  and  $Q_5$  we have  $x_{bs}^{-1} \sim Q_i / R^2$  where  $Q_i$  is the smaller of the two. In other words, the size of the bound state is strongly dependent on the background. When the charges are large, the bound state will be mostly contained within the ergoregion, while for small charges the exponential tail of the bound state can extend far outside.

Finally we can consider the possibility that the bound states have negative energy, which requires a detailed analysis of the energy integral (7). Examining the integrand evaluated on bound state solutions, we see that it may become negative near where the modulus of the scalar field peaks if the latter occurs inside the ergoregion. Though there are bound states for arbitrarily large values of  $|\lambda|$ , the total energy will not be negative for all of these. Instead, the modes that tend to exhibit negative energy densities (in the ergoregion) only appear for a limited range of  $|\lambda|$ , which is just beyond the small- $|\lambda|$  regime discussed above. That is, for values of  $\lambda$  near where the ergoregion instability appears. When this is the case, the maximum of the modulus of the scalar field is inside the ergoregion and the phase velocity in the compactified direction  $\Sigma_y = \omega/\lambda$  is negative, *i.e.*, in the direction opposite to which the background is boosted.

- 
- [1] V. Jejjala, O. Madden, S.F. Ross and G. Titchener, “Non-supersymmetric smooth geometries and D1-D5-P bound states,” Phys. Rev. D **71**, 1240030 (2005), hep-th/0504181.
- [2] A. Strominger and C. Vafa, “Microscopic Origin of the Bekenstein-Hawking Entropy,” Phys. Lett. B **379** (1996) 99, hep-th/9601029.
- [3] A.W. Peet, “The Bekenstein formula and string theory (N-brane theory),” Class. Quant. Grav. **15** (1998) 3291, hep-th/9712253;  
S.R. Das and S.D. Mathur, “The quantum physics of black holes: Results from string theory,” Ann. Rev. Nucl. Part. Sci. **50** (2000) 153, gr-qc/0105063;  
J.R. David, G. Mandal and S.R. Wadia, “Microscopic formulation of black holes in string theory,” Phys. Rept. **369** (2002) 549, hep-th/0203048.
- [4] J. M. Maldacena, “The large N limit of superconformal field theories and supergravity,” Adv. Theor. Math. Phys. **2** (1998) 231, hep-th/9711200;  
E. Witten, “Anti-de Sitter space and holography,” Adv. Theor. Math. Phys. **2** (1998) 253, hep-th/9802150.
- [5] O. Aharony, S.S. Gubser, J.M. Maldacena, H. Ooguri and Y. Oz, “Large N field theories, string theory and gravity,” Phys. Rept. **323** (2000) 183, hep-th/9905111.
- [6] E. Witten, “Anti-de Sitter space, thermal phase transition, and confinement in gauge theories,” Adv. Theor. Math. Phys. **2** (1998) 505, hep-th/9803131.
- [7] A. Chamblin, R. Emparan, C.V. Johnson and R.C. Myers, “Holography, thermodynamics and fluctuations of charged AdS black holes,” Phys. Rev. D **60** (1999) 104026, hep-th/9904197.
- [8] R. Dijkgraaf, J.M. Maldacena, G.W. Moore and E.P. Verlinde, “A black hole farey tail,” hep-th/0005003.
- [9] R.C. Myers, “Pure states don’t wear black,” Gen. Rel. Grav. **29** (1997) 1217, gr-qc/9705065.
- [10] D. Amati, “Black holes, string theory and quantum coherence,” Phys. Lett. B **454** (1999) 203, hep-th/9706157.
- [11] S.D. Mathur, “The fuzzball proposal for black holes: An elementary review,” Fortsch. Phys. **53** (2005) 793, hep-th/0502050;  
S.D. Mathur, “The quantum structure of black holes,” hep-th/0510180.
- [12] O. Lunin and S.D. Mathur, “Statistical interpretation of Bekenstein entropy for systems with a stretched horizon,” Phys. Rev. Lett. **88** (2002) 211303, hep-th/0202072.
- [13] O. Lunin and S.D. Mathur, “AdS/CFT duality and the black hole information paradox,” Nucl. Phys. B **623** (2002) 342, hep-th/0109154.
- [14] O. Lunin and S.D. Mathur, “The slowly rotating near extremal D1-D5 system as a ‘hot tube,’” Nucl. Phys. B **615** (2001) 285, hep-th/0107113.
- [15] V. Balasubramanian, J. de Boer, E. Keski-Vakkuri, and S. F. Ross, “Supersymmetric conical defects: Towards a string theoretic description of black hole formation,” Phys. Rev. D **64** (2001) 064011, hep-th/0011217;  
J. M. Maldacena and L. Maoz, “De-singularization by rotation,” JHEP **12** (2002) 055, hep-th/0012025;  
O. Lunin and S. D. Mathur, “Metric of the multiply wound rotating string,” Nucl. Phys. B **610** (2001) 49, hep-th/0105136;  
O. Lunin, J. Maldacena, and L. Maoz, “Gravity solutions for the D1-D5 system with angular momentum,” hep-th/0212210;  
M. Taylor, “General 2 charge geometries,” hep-th/0507223.

- [16] A.A. Tseytlin, “Extreme dyonic black holes in string theory,” *Mod. Phys. Lett. A* **11** (1996) 689, hep-th/9601177;  
J.C. Breckenridge, R.C. Myers, A.W. Peet and C. Vafa, “D-branes and spinning black holes,” *Phys. Lett. B* **391** (1997) 93, hep-th/9602065.
- [17] J.C. Breckenridge, D.A. Lowe, R.C. Myers, A.W. Peet, A. Strominger and C. Vafa, “Macroscopic and Microscopic Entropy of Near-Extremal Spinning Black Holes,” *Phys. Lett. B* **381** (1996) 423, hep-th/9603078;  
M. Cvetič and D. Youm, “General Rotating Five Dimensional Black Holes of Toroidally Compactified Heterotic String,” *Nucl. Phys. B* **476** (1996) 118, hep-th/9603100.
- [18] O. Lunin, “Adding momentum to D1-D5 system,” *JHEP* **0404** (2004) 054, hep-th/0404006.
- [19] S. Giusto, S. D. Mathur, and A. Saxena, “Dual geometries for a set of 3-charge microstates,” *Nucl. Phys. B* **701** (2004) 357-379, hep-th/0405017.
- [20] S. Giusto, S. D. Mathur, and A. Saxena, “3-charge geometries and their CFT duals,” *Nucl. Phys. B* **710** (2005) 425-463, hep-th/0406103;  
I. Bena and N.P. Warner, “One ring to rule them all ... and in the darkness bind them?,” hep-th/0408106;  
I. Bena and N.P. Warner, “Bubbling supertubes and foaming black holes,” hep-th/0505166;  
P. Berglund, E.G. Gimon and T.S. Levi, “Supergravity microstates for BPS black holes and black rings,” hep-th/0505167.
- [21] I. Bena and P. Kraus, “Microstates of the D1-D5-KK system,” *Phys. Rev. D* **72** (2005) 025007, hep-th/0503053;  
I. Bena, P. Kraus and N.P. Warner, “Black rings in Taub-NUT,” *Phys. Rev. D* **72** (2005) 084019, hep-th/0504142;  
H. Elvang, R. Emparan, D. Mateos and H.S. Reall, “Supersymmetric 4D rotating black holes from 5D black rings,” *JHEP* **0508** (2005) 042, hep-th/0504125;  
A. Saxena, G. Potvin, S. Giusto and A.W. Peet, “Smooth geometries with four charges in four dimensions,” hep-th/0509214.
- [22] W.H. Press and S.A. Teukolsky, “Floating Orbits, super-radiant scattering and the black-hole bomb,” *Nature* **238** (1972) 211.
- [23] T. Damour, N. Deruelle and R. Ruffini, “On Quantum Resonances In Stationary Geometries,” *Lett. Nuovo Cim.* **15** (1976) 257.
- [24] V. Cardoso, O.J.C. Dias, J.P.S. Lemos and S. Yoshida, “The black hole bomb and superradiant instabilities,” *Phys. Rev. D* **70** (2004) 044039, hep-th/0404096 [Erratum-ibid. *D* **70** (2004) 049903].
- [25] Ya.B. Zel’dovich, *Pis’ma Zh. Eksp. Teor. Fiz.* **14**, 270 (1971) [*JETP Lett.* **14**, 180 (1971)];  
Ya.B. Zel’dovich, “Amplification of cylindrical electromagnetic waves reflected from a rotating body,” *Zh. Eksp. Teor. Fiz.* **62**, 2076 (1972) [*Sov. Phys. JETP* **35**, 1085 (1972)].
- [26] J.L. Friedman, “Ergosphere instability,” *Commun. Math. Phys.* **63**, 243 (1978).
- [27] N. Comins and B.F. Schutz, “On the ergoregion instability,” *Proc. R. Soc. Lond. A* **364** (1978) 211.
- [28] S. Yoshida and E. Eriguchi, “Ergoregion instability revisited – a new and general method for numerical analysis of stability,” *MNRAS* **282** (1996) 580.
- [29] S.F. Ross, “Winding tachyons in asymptotically supersymmetric black strings,” hep-th/0509066.
- [30] G.T. Horowitz, “Tachyon condensation and black strings,” *JHEP* **0508** (2005) 091, hep-th/0506166.
- [31] S. Detweiler, “Klein-Gordon Equation And Rotating Black Holes,” *Phys. Rev. D* **22** (1980) 2323.
- [32] V. Cardoso and O. J. C. Dias, “Small Kerr-anti-de Sitter black holes are unstable,” *Phys. Rev. D* **70** (2004) 084011, hep-th/0405006.
- [33] V. Cardoso and S. Yoshida, “Superradiant instabilities of rotating black branes and strings,” *JHEP* **0507** (2005) 009, hep-th/0502206.
- [34] M. Cvetič and F. Larsen, “General rotating black holes in string theory: Greybody factors and event horizons,” *Phys. Rev. D* **56** (1997) 4994, hep-th/9705192.
- [35] Four-dimensional spin-weighted spheroidal harmonics were introduced in:  
S.A. Teukolsky, “Perturbations Of A Rotating Black Hole. 1. Fundamental Equations For Gravitational, Electromagnetic, And Neutrino Field Perturbations,” *Astrophys. J.* **185** (1973) 635.  
The generalization to higher dimensions can be found in:  
V.P. Frolov and D. Stojkovic, “Quantum radiation from a 5-dimensional rotating black hole,” *Phys. Rev. D* **67** (2003) 084004, gr-qc/0211055;  
V. P. Frolov and D. Stojkovic, “Particle and light motion in a space-time of a five-dimensional rotating black hole,” *Phys. Rev. D* **68**, 064011 (2003), gr-qc/0301016;  
M. Vasudevan, K. A. Stevens and D. N. Page, “Particle motion and scalar field propagation in Myers-Perry black hole spacetimes in all dimensions,” *Class. Quant. Grav.* **22** (2005) 1469, gr-qc/0407030.
- [36] R.C. Myers and M.J. Perry, “Black Holes In Higher Dimensional Space-Times,” *Annals Phys.* **172** (1986) 304.
- [37] A.A. Starobinsky, *Sov. Phys. JETP* **37** (1973) 28;  
A.A. Starobinsky and S.M. Churilov, “Amplification of electromagnetic and gravitational waves scattered by a rotating black hole,” *Sov. Phys. JETP* **38** (1973) 1;  
W. G. Unruh, “Absorption cross-section of small black holes,” *Phys. Rev. D* **14** (1976) 3251.
- [38] V. Cardoso, O.J.C. Dias and S. Yoshida, “Perturbations and absorption cross-section of infinite-radius black rings,” *Phys. Rev. D* **72** (2005) 024025, hep-th/0505209.
- [39] M. Abramowitz and A. Stegun, *Handbook of mathematical functions*, (Dover Publications, New York, 1970).
- [40] Wolfram Research, Inc., *Mathematica*, Version 5.0, Champaign, IL (2003).
- [41] E. Witten, “Instability Of The Kaluza-Klein Vacuum,” *Nucl. Phys. B* **195** (1982) 481;  
D. Brill and G.T. Horowitz, “Negative energy in string theory,” *Phys. Lett. B* **262** (1991) 437;  
D. Brill and H. Pfister, “States Of Negative Total Energy In Kaluza-Klein Theory,” *Phys. Lett. B* **228** (1989) 359.

- [42] C.G. Callan and J.M. Maldacena, “D-brane Approach to Black Hole Quantum Mechanics,” Nucl. Phys. B **472** (1996) 591, hep-th/9602043.
- [43] J.M. Maldacena and A. Strominger, “Black hole greybody factors and D-brane spectroscopy,” Phys. Rev. D **55** (1997) 861, hep-th/9609026.
- [44] S.R. Das and S.D. Mathur, “Comparing decay rates for black holes and D-branes,” Nucl. Phys. B **478** (1996) 561, hep-th/9606185;  
S.R. Das and S.D. Mathur, “Interactions involving D-branes,” Nucl. Phys. B **482** (1996) 153, hep-th/9607149.
- [45] G.T. Horowitz and A. Strominger, “Counting States of Near-Extremal Black Holes,” Phys. Rev. Lett. **77** (1996) 2368, hep-th/9602051;  
J.C. Breckenridge, D.A. Lowe, R.C. Myers, A.W. Peet, A. Strominger and C. Vafa, “Macroscopic and Microscopic Entropy of Near-Extremal Spinning Black Holes,” Phys. Lett. B **381** (1996) 423, hep-th/9603078.
- [46] J.M. Maldacena, “D-branes and near extremal black holes at low energies,” Phys. Rev. D **55** (1997) 7645, hep-th/9611125.
- [47] V. Cardoso, O.J.C. Dias, J.L. Hovdebo and R.C. Myers, in preparation.
- [48] D. Marolf and B.C. Palmer, “Gyrating strings: A new instability of black strings?,” Phys. Rev. D **70** (2004) 084045, hep-th/0404139.
- [49] R. Gregory and R. Laflamme, “Black strings and p-branes are unstable,” Phys. Rev. Lett. **70** (1993) 2837, hep-th/9301052;  
R. Gregory and R. Laflamme, “The Instability of charged black strings and p-branes,” Nucl. Phys. B **428** (1994) 399, hep-th/9404071.
- [50] J.L. Hovdebo and R.C. Myers, “Black Rings, Boosted Strings and Gregory-Laflamme,” in preparation.
- [51] R. Emparan and R.C. Myers, “Instability of ultra-spinning black holes,” JHEP **0309** (2003) 025, hep-th/0308056.
- [52] R. Emparan and H.S. Reall, “A rotating black ring in five dimensions,” Phys. Rev. Lett. **88** (2002) 101101, hep-th/0110260.
- [53] V. Balasubramanian, P. Kraus and M. Shigemori, “Massless black holes and black rings as effective geometries of the D1-D5 system,” Class. Quant. Grav. **22** (2005) 4803, hep-th/0508110.
- [54] O. Lunin and S.D. Mathur, “Three-point functions for M(N)/S(N) orbifolds with N = 4 supersymmetry,” Commun. Math. Phys. **227** (2002) 385, hep-th/0103169.
- [55] H. Lin, O. Lunin and J. Maldacena, “Bubbling AdS space and 1/2 BPS geometries,” JHEP **0410** (2004) 025, hep-th/0409174;  
S. Corley, A. Jevicki and S. Ramgoolam, “Exact correlators of giant gravitons from dual N = 4 SYM theory,” Adv. Theor. Math. Phys. **5** (2002) 809, hep-th/0111222.  
D. Berenstein, “A toy model for the AdS/CFT correspondence,” JHEP **0407** (2004) 018, hep-th/0403110.
- [56] D. Martelli and J.F. Morales, “Bubbling AdS(3),” JHEP **0502** (2005) 048, hep-th/0412136;  
J.T. Liu, D. Vaman and W.Y. Wen, “Bubbling 1/4 BPS solutions in type IIB and supergravity reductions on  $S^n \times S^n$ ,” hep-th/0412043;  
J.T. Liu and D. Vaman, “Bubbling 1/2 BPS solutions of minimal six-dimensional supergravity,” hep-th/0412242.
- [57] G. Mandal, “Fermions from half-BPS supergravity,” JHEP **0508** (2005) 052, hep-th/0502104;  
L. Grant, L. Maoz, J. Marsano, K. Papadodimas and V.S. Rychkov, “Minisuperspace quantization of ‘bubbling AdS’ and free fermion droplets,” JHEP **0508** (2005) 025, hep-th/0505079;  
L. Maoz and V.S. Rychkov, “Geometry quantization from supergravity: The case of ‘bubbling AdS’,” JHEP **0508** (2005) 096, hep-th/0508059.
- [58] A. Jevicki and A. Donos, “Dynamics of chiral primaries in  $AdS_3 \times S^3 \times T^4$ ,” hep-th/0512017;  
V.S. Rychkov, “D1-D5 black hole microstate counting from supergravity,” hep-th/0512053.
- [59] D. Berenstein, “Large N BPS states and emergent quantum gravity,” hep-th/0507203;  
P.G. Shepard, “Black hole statistics from holography,” JHEP **0510** (2005) 072, hep-th/0507260;  
V. Balasubramanian, J. de Boer, V. Jejjala and J. Simon, “The library of Babel: On the origin of gravitational thermodynamics,” hep-th/0508023;  
V. Balasubramanian, V. Jejjala and J. Simon, “The library of Babel,” hep-th/0505123;  
P.J. Silva, “Rational foundation of GR in terms of statistical mechanics in the AdS/CFT framework,” hep-th/0508081.